Report no. changed (Mar 2006): SR-220-UU

SACLANTCEN REPORT
serial no.: SR-220

SACLANT UNDERSEA
RESEARCH CENTRE

REPORT

Sea-surface winds in the Iceland–Faeroe area, as derived from the ERS-1 scatterometer

H.-H. Essen

April 1994

Report no. changed (Mar 2006): SR-220-UU

This document is released to a NATO Government at the direction of SACLANT Undersea Research Centre subject to the following conditions:

- The recipient NATO Government agrees to use its best endeavours to ensure that the information herein disclosed, whether or not it bears a security classification, is not dealt with in any manner (a) contrary to the intent of the provisions of the Charter of the Centre, or (b) prejudicial to the rights of the owner thereof to obtain patent, copyright, or other like statutory protection therefor.
- If the technical information was originally released to the Centre by a NATO Government subject to restrictions clearly marked on this document the recipient NATO Government agrees to use its best endeavours to abide by the terms of the restrictions so imposed by the releasing Government.

Page count for SR-220 (excluding Covers and Data Sheet)

Pages	Total
i–vi	6
1–54	54
	60

SACLANT Undersea Research Centre
Viale San Bartolomeo 400
19138 San Bartolomeo (SP), Italy

tel: 0187 540 111
fax: 0187 524 600
telex: 271148 SACENT I

NORTH ATLANTIC TREATY ORGANIZATION

Report no. changed (Mar 2006): SR-220-UU

SACLANTCEN SR-220

Sea-surface winds in the Iceland–Faeroe area, as derived from the ERS-1 scatterometer

H.-H. Essen

The content of this document pertains to work performed under Project 23 of the SACLANTCEN Programme of Work. The document has been approved for release by The Director, SACLANTCEN.

David L. Bradley
Director

intentionally blank page

Report no. changed (Mar 2006): SR-220-UU

SACLANTCEN SR-220

Sea-surface winds in the Iceland–Faeroe area, as derived from the ERS-1 scatterometer

H.-H. Essen

Executive Summary: In the past, satellite remote sensing at SACLANTCEN has concentrated on the retrieval of sea-surface temperatures from spaceborne radiometers. Data from the Advanced Very High Resolution Radiometer (AVHRR) have been available for some fifteen years from the series of NOAA satellites. The main disadvantage of infrared radiometry for oceanographic applications is the requirement for a cloud-free sky. As oceanographic research of SACLANTCEN has been dealing with the Iceland–Faeroe Frontal (IFF) region this constraint is of considerable importance. Microwave sensors are less affected by the intervening atmosphere and promise a weather-independent monitoring of the ocean's surface. Since summer 1991, the European Remote Sensing Satellite (ERS-1) has been in orbit, carrying a number of microwave sensors especially designed for oceanic applications.

SACLANTCEN submitted a proposal 'Modelling of the Ocean with Remote Sensing from ERS-1' (MORSE) to the European Space Agency (ESA). The principal objective of MORSE is to use ERS-1 data in conjunction with numerical ocean circulation models. Specific aims are to describe the large and mesoscale circulation and to determine the configuration and variability of fronts, mainly the IFF. As a first step, selected oceanographic variables measured by ERS-1 are compared with the corresponding data from conventional *in situ* measurements, in order to study the error characteristics of the satellite data. This report deals with the wind scatterometer of ERS-1, which is an active microwave radar designed to monitor surface winds.

The ability to measure worldwide sea-surface winds over large ocean areas is of great importance to many scientific and operational purposes. The present report shows that, from the new C-band scatterometer of ERS-1, wind speeds may be determined with an accuracy of about ± 2 ms^{-1}. This result has been found by comparing scatterometer-retrieved winds with a limited number of *in situ* winds measured from on board R/V *Alliance* and with analysed winds from the archive of the UK Meteorological Office. It has also been found that in the presence of snow showers real winds are considerably underestimated by the scatterometer. Particularly for the IFF area this is of importance, because snow- or rain-fall is a frequent phenomena there.

In the future, SACLANTCEN will concentrate oceanographic investigations in the shallow-water coastal areas of the Mediterranean. Because of the limited resolution of the scatterometer (50 km), it is not a very useful instrument for this purpose. In addition to the AVHRR the remote sensing work will take advantage of the Synthetic Aperture Radar (SAR), which can be considered as a high-resolution scatterometer.

intentionally blank page

Report no. changed (Mar 2006): SR-220-UU

SACLANTCEN SR-220

Sea-surface winds in the Iceland–Faeroe area, as derived from the ERS-1 scatterometer

H.-H. Essen

Abstract: This report presents measurements of surface meteorological data taken during three cruises of R/V *Alliance* to the Iceland–Faeroe frontal area during August 1991 (NORDIC'91), March 1992 (NORDIC'92a) and October 1992 (NORDIC'92b). Wind velocity and direction, as measured at three different locations on the ship, are compared with wind information retrieved from the scatterometer of the European Remote Sensing Satellite (ERS-1). As coincident *in situ* and satellite measurements are relatively rare, analysed winds from the UK Meteorological Office are also used for comparison. For the satellite data, different retrieval algorithms are applied. Beside the wind vector, its horizontal derivatives (e.g. horizontal divergence and curl) are also investigated.

Keywords: ERS-1 ○ Iceland–Faeroe area ○ microwave radar ○ satellite remote sensing ○ scatterometer ○ sea-surface winds

Contents

Acknowledgements: Thanks go to P. Minnett who introduced me to the ZAN data collecting system on board of R/V *Alliance*, to M. Zahorodny who helped with the software, and D. Galletti and R. Della Maggiore who installed the system and performed the calibration. The scatterometer data were supplied by the European Space Agency (ESA) and the analysed wind data by the UK Meteorological Office.

1 Introduction

Satellite remote sensing offers the possibility of observing large areas of the ocean quasi-synoptically. ERS-1, launched in summer 1991, is primarily orientated towards ocean monitoring, and carries instrumentation consisting mainly of active microwave sensors. These have the advantage of being independent of daylight and of not being affected by cloud coverage. The Active Microwave Instrumentation (AMI) combines a Synthetic Aperture Radar (SAR) with a Wind Scatterometer (SCAT). This report deals with the SCAT only.

The circulation of the ocean is primarily wind-driven, and reliable wind fields are required for oceanic modelling. Space-borne scatterometers are able to contribute information on wind speed and direction with a resolution of about 50 km on a swath of about 500 km width. SCAT measures the normalised radar cross section σ_0 by means of three antennas which successively view the same surface element under three different look angles. The retrieval of wind velocity is based on the dependence of σ_0 on ocean roughness, which itself depends on surface winds. σ_0 is anisotropic with respect to the angle between wind vector and incident radar beam. With the aid of several σ_0 measurements of the same area from different directions, the surface wind vector can be determined in terms of speed and direction.

A number of physical processes affect the retrieval of wind at a certain reference level (usually 10 m) from measured radar cross sections. The most important are, radar backscatter from a rough sea surface, generation of surface waves by wind, and the structure of the atmosphere between the sea surface and the reference level. These processes are rather complex, and no quantitatively reliable theory exists, which includes all the influences mentioned. Instead, the dependence of σ_0 on the wind vector has been studied in a number of radar backscattering experiments carried out from from aircraft (e.g. Feindt et al., 1986) or sea-based platforms (e.g. Keller et al., 1989). These experiments show some evidence that σ_0 is not only a function of the local wind but also of other environmental parameters such as the air-sea temperature difference and wave slopes.

The radar scatterometer on board of SEASAT, in operation for 100 days during 1978, proved the value of this instrument (Guymer, 1987). Algorithms could be developed for reliably retrieving wind fields, covering the oceans worldwide. SCAT of ERS-1 differs in two aspects from the SEASAT scatterometer, each surface element is viewed by three antenna beams of different direction instead of two, and the radar frequency is 5.3 GHz instead of 14.6 GHz. The latter difference is of special importance, because it means that the empirical relations found for SEASAT are

not appliable for ERS-1. Retrieval algorithms for SCAT have been developed by using data from air-borne and tower-mounted scatterometers.

Wind data as collected by R/V *Alliance* during cruises in the Iceland–Faeroe Frontal (IFF) area are reported here and compared with satellite data. The schedule of the oceanographic ship cruises could not be coordinated with satellite overpasses. For this reason, the number of coincident satellite and *in situ* measurements is limited. In addition, the SCAT was not correctly calibrated during NORDIC'91 (August 1991), and recalibrated data are not yet available. During NORDIC'92a (March 1992), intensive use was made of the SAR in the IFF area, which excludes the operation of SCAT. In total, only data from ten coincident measurements are available, five each from NORDIC'92a and NORDIC'92b (October 92). For this reason, analysed winds from the wind archive of the UK Meteorological Office (UKMO) are also used for comparison with both wind velocities measured on R/V *Alliance* and retrieved from the SCAT.

The present report is thought to support the validation efforts of ESA in an area of special interest to SACLANTCEN. The IFF area is an open-sea region of high oceanographic and meteorological variability. The *in situ* data available contain different meteorological situations, low and high wind speeds, and stable and unstable atmospheric boundary layers with the air-sea temperature difference falling below $-10\,^{\circ}\mathrm{C}$. Another aim of this report is to explore the value of the SCAT data for oceanographic modelling. Satellite measured winds are supposed to yield more reliable forcing in numerical ocean models than the considerably smoothed analysed data from meteorological services.

2

Wind retrieval from scatterometer data

This section briefly describes the scatterometer on ERS-1 and discusses the physical processes which affect the retrieval of wind velocities at a certain reference height from satellite-measured radar cross sections. These are the backscatter of electromagnetic waves in the microwave bands from a rough sea surface, the generation of surface roughness by wind, and the dependence of wind speed on altitude in the atmospheric boundary layer. Also, some aspects of retrieval algorithms are discussed. More details on this subject are presented in Appendix A.

2.1. SCATTEROMETER OF ERS-1

ERS-1 was launched in July 91. The standard altitude of the sun synchronous near polar orbit is 785 km, the inclination 98.52°and the period about 100 min. The AMI, combining the SAR and the SCAT, operates at 5.3 GHz (C-band) with vertical polarisation for both transmitting and receiving. The SCAT illuminates the sea surface sequentially by radio pulses from three antennas pointing in different azimuthal directions, 45°, 90° and 135° with respect to the satellite track. The ranges of incident angle at the sea surface are 18–47° for the mid-antenna and 25–59° for the forward- and backward-looking antennas. This geometry allows radar echoes to be received from a 500 km wide swath along the satellite track. As the satellite advances, each point within the swath is successively viewed from the three different azimuth angles. Normalized radar cross sections are deduced at nodes with 25 km separation. Each node is centred within a resolution cell of 50 km $\times$ 50 km, which is determined in range direction by appropriate range gating of the backscattered signal and in azimuth by averaging of corresponding range-gated signals from successive pulses. The pulse width for the mid-antenna is 70 μs and 130 μs for the other two. Each cell is illuminated by 128 pulses of each antenna.

By on-board and on-ground signal processing the normalised radar backscattering coefficients σ_0 and the x- and y-coordinates corresponding to the along- and cross-track position are produced. In addition, ESA supplies the results of their wind retrieval, consisting of an array of wind vectors expressed in wind speed and direction. The product corresponds to a 500 km $\times$ 500 km area, which is represented by a 19 $\times$ 19 array of cells, with 25 km nominal spacing. The wind field produced corresponds to an equivalent neutral stability wind field, referenced to a height of 10 m.

2.2. BRAGG SCATTERING

As generally accepted, resonant Bragg scattering is the dominant process generating radar backscatter in the range of incident angles as used by SCAT, i.e. from 18–59°. For smaller incident angles, specular reflection from sloping surface elements has to be taken into account and for larger incident angles shadowing effects become important. The condition for Bragg scattering reads

$$\mathbf{k}_s = \pm 2\mathbf{k}_r \qquad \text{with} \qquad \mathbf{k}_r = \frac{2\pi\nu}{c}(\sin\varphi, \cos\varphi)\sin\vartheta, \tag{1}$$

where ν is the frequency of the radar, c the velocity of light, φ and ϑ are the azimuthal and incident angle of the radar beam, respectively, and $\mathbf{k}_s$ is the two-dimensional vector of surface waves responsible for backscattering. Thus backscattering is due to surface waves with wavelengths $\lambda_s = c/(2\nu\sin\vartheta)$, travelling parallel or antiparallel to the horizontal projection of the radar beam. For the frequency and incident angles of SCAT, the range of scattering surface wavelengths extends from 3.3 cm to 9.2 cm.

The theory of Bragg scattering determines the relation of the normalised radar cross section to the two-dimensional wavenumber spectrum $F(\mathbf{k}_s)$ of sea surface waves, cf. Wright (1968),

$$\sigma_0 = T(\nu, \vartheta)\{F(2\mathbf{k}_r) + F(-2\mathbf{k}_r)\}, \tag{2}$$

where in addition, the coefficient T depends on the permittivity of the water illuminated and on the polarisation of the transmitted and received signals, which both are vertical for the SCAT.

Relying on Eq. (2), we will shortly discuss the main difficulties in retrieving sea-surface winds from σ_0, as measured by radar. First it has to be assumed that the two-dimensional roughness spectrum depends on the horizontal vector of surface winds, which obviously is the case. But on the other hand, no quantitatively accurate theory based on physical laws is yet available. In addition, little is known about the short-wave spectrum, especially regarding its angular dependence. Experimental investigations are hard to perform and are rare for this reason.

Beside the local wind, other environmental influences may considerably modify the wave spectrum in Eq. (2). Radar scatter is due to short surface waves (ripples), the dynamics of which are significantly influenced by underlying long waves (hydrodynamical modulation). Indeed, due to this modulation the high-resolution SAR is able to image ocean swell. The theoretical concept of the 'modulation transfer function' directly relates (in wavenumber space) the variations of the radar cross section to long surface waves. The tower-based experiments of Keller et al. (1989) showed an increase of σ_0 with increasing rms wave slope at low wind speeds for stable boundary layers. Space-borne scatterometers illuminate an area large compared to even the swell wavelength and it may be assumed that part of the dependence on long waves averages out.

Natural or man-made films on the sea surface cause an attenuation of sea-wave amplitudes and may considerably decrease σ_0, cf. Hühnerfuss et al. (1981). With

respect to our data, which are from the IFF area in March and October, this effect may assumed to be of less importance. By interpreting SEASAT scatterometer data, Guymer (1987) discusses the influence of rain. Rainfall normally is expected to decrease the spectral amplitudes and thus σ_0, but in the case of a very smooth surface it also may account for the opposite effect.

Returning to the generation of waves by wind, it may be stated that the physical processes involved are not yet understood (cf. Pond and Pickard, 1983). In the case of an ideally smooth surface, momentum is tranferred from the atmosphere to the upper water layer by molecular viscous shear stress. The thickness of the atmospheric layer involved is of the order of 1 mm and this process is of only little importance. If the surface already contains some roughness, the bumps on the surface will cause the air flow to produce pressure differences between upwind and downwind sides of the wave crests, and stress tranfer may occur due to these pressure differences or what is called 'form drag'. As pressure is a normal stress, the final transfer is mainly by normal rather than shear stresses. This assumption is confirmed by the fact that surface waves are irrotational and thus produced by normal stresses.

2.3. ATMOSPHERIC BOUNDARY LAYER

The interest in the atmospheric boundary layer is twofold. Surface winds are normally referred to a certain level above the sea surface, which is usually 10 m. Winds from deviating levels, as obtained from measurements on board R/V *Alliance* or from numerical weather analysis, have to be adjusted to the standard level, which requires knowledge on the wind profile. The second interest concerns the retrieval of winds at the 10 m level from σ_0 as measured by the scatterometer. Radar backscatter is due to the roughness at the surface, and it may be expected that the intervening atmosphere influences the wind velocity at the reference height of 10 m. Scatterometer retrieved winds refer to neutral stability of the atmospheric boundary layer, i.e. for comparison with other wind data, these have to be corrected for stability, which is mainly determined by the air-water temperature difference.

Reviews of theoretical and empirical knowledge concerning the atmospheric surface layer are given by e.g. Charnock (1981) and Stewart (1985), the latter more orientated for remote sensing applications. Turbulence as generated by wind shear is the dominating process within the atmospheric boundary layer, which extends to some 20–50 m above sea level. Molecular processes are important only within about the first 1 mm above the air/sea interface. Mainly because of difficulties due to surface waves, the boundary conditions at the sea surface are not yet understood, and most theoretical investigations are based on dimensional arguments. Though the generation of surface waves is most probably due to density fluctuations, the primary momentum source for wave growth is the wind stress τ, which is assumed to be independent of height in the atmospheric boundary layer,

$$\tau = \rho_a \{ \langle u'w' \rangle , \langle v'w' \rangle \}, \tag{3}$$

where ρ_a is the density of air and (u', v', w') are the perturbations of the three components of wind velocity about their mean values. The angle brackets denote mean values. The wind stress and the mean wind velocity $\mathbf{U}$ at a certain height are assumed to be related by the bulk formula,

$$\boldsymbol{\tau} = \rho_a C_D U \mathbf{U}, \tag{4}$$

where C_D is the drag coefficient. If the potential density is independent of height (neutral stability) the vertical gradient of the wind velocity $\mathrm{d}U/\,\mathrm{d}z$ is found to vary quite accurately to the inverse of height, yielding a logarithmic profile of mean wind speed versus height. This dependence is predicted by dimension analysis and holds for heights starting just above the crests of surface roughness.

In unstable conditions, i.e. potential density increasing with height, turbulence increases and as does its ability to transfer momentum. In stable conditions the converse is true. Stability may be defined by means of the Monin-Obukhov length L, which estimates the height of bouyancy forces becoming as important as shear forces. Assuming that the sensible heat transfer coefficient is approximately equal to the drag coefficient, L becomes, cf. Smith (1988),

$$L = -\frac{T_w u_*^3}{\kappa g C_D U (T_w - T_a)}, \qquad u_*^2 = C_D U^2, \tag{5}$$

where u_* is the friction velocity, T_a and T_w (measured in K) are the temperatures of air and water, respectively. $\kappa = 0.4$ is the Karman constant, and $g = 9.8\ \mathrm{ms}^{-2}$, the gravity acceleration.

The logarithmic profile of wind velocity for neutral conditions has to be corrected by a stability function ψ depending on z/L in the case of stable or unstable conditions,

$$U(z) = \frac{u_*}{\kappa}[\ln \frac{z}{z_0} - \psi(\frac{z}{L})], \tag{6}$$

where z_0 is the roughness height, which is assumed to be, cf. Smith (1988),

$$z_0 = 0.011 \frac{u_*^2}{g}, \tag{7}$$

i.e. proportional to the wind stress. The stability function, determined from various experiments in the open sea may be represented by, cf. Smith (1988),

$$\psi = -5.0 \frac{z}{L} \qquad \text{if} \qquad \frac{z}{L} > 0 \quad \text{(stable)}$$

$$\psi = 2 \ln \frac{1+x}{2} + \ln \frac{1+x^2}{2} - 2 \tan^{-1} x + \frac{\pi}{2} \qquad \text{if} \qquad \frac{z}{L} < 0 \quad \text{(unstable)},$$

with

$$x = (1 - 16\frac{z}{L})^{\frac{1}{4}}, \tag{8}$$

Equations (5–8) implicitly determine C_D for a given wind speed at height z and the temperature difference $T_a - T_w$. Assuming the temperature difference to be independent of height, C_D is determined by means of a search algorithm. Smith (1988) also takes the temperature profile into account and presents C_D values for the reference height of 10 m. His results are well reproduced by our simplified method.

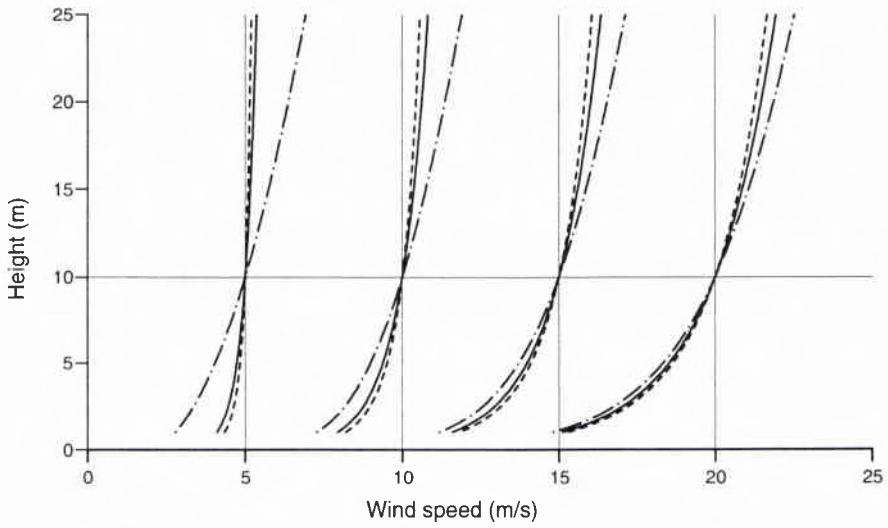

Figure 1 *Wind-velocity profiles with fixed speeds at 10 m height, for different atmospheric boundary layers: dashed lines, $T_a - T_w = -6\,°C$ (unstable); solid lines, $T_a - T_w = 0\,°C$ (neutral); dashed-dotted lines, $T_a - T_w = +6\,°C$ (stable).*

Figure 1 displays profiles of the mean wind speed as computed from Eqs. (5–8). In order to show the influence of stability on the atmospheric boundary layer the profiles pass through fixed speeds at the reference height of 10 m. The wind speed near the sea surface becomes greater for unstable rather than for stable conditions, with larger deviations for low rather than for high wind speeds. This explains why σ_0 is larger for an unstable boundary layer than for a stable one, as found by Keller et al. (1989) in their tower-based experiment.

Wind data available for comparison with scatterometer-retrieved winds are usually not from the reference height of 10 m. *In situ* measured winds on board R/V *Alliance* are from 12 m and 16 m above sea level. The analysed winds of the UKMO refer to 25 m height. Information about the stability of the atmospheric boundary layer is available for the *in situ* and the respective analysed winds. In this case, wind speeds are adjusted to neutral conditions and to 10 m height. This is done by computing the drag coefficient C_D as described, which determines the (height-independent) friction

velocity u_* by Eq. (5). First the wind speed $U(z)$ is corrected to the value it would have at neutral conditions $U_n(z)$ at the same height, cf. Eq. (6),

$$U_n(z) = U(z) + \frac{u_*}{\kappa}\psi(\frac{z}{L}). \tag{9}$$

Then the logarithmic profile is used to find the wind speed U_{10} at the reference height,

$$U_{10} = U_n(z) - \frac{u_*}{\kappa}\ln(\frac{z}{10\text{ m}}). \tag{10}$$

If no information on the air-sea temperature is available, a neutral boundary layer is assumed. i.e. $U_n(z) = U(z)$, and only (10) is applied for correction. Considering the measured heights of interest and a wind speed of 10 ms^{-1}, (10) yields

$$U_n(10\text{ m}) = \begin{cases} 0.984 \times U_n(12\text{ m}), \\ 0.960 \times U_n(16\text{ m}), \\ 0.924 \times U_n(25\text{ m}). \end{cases} \tag{11}$$

The proportionality factors show only little variation with wind speed and are used for correcting to the reference height.

2.4. RETRIEVAL ALGORITHM

The determination of winds by measuring radar backscatter is based on the σ_0 model, which describes the dependence of σ_0 on the wind vector characterised by speed U and direction φ (defined meteorologically as the direction from which the wind is blowing). The retrieved winds correspond to an equivalent neutral stratification of the atmospheric boundary layer and to a height of 10 m above sea level. Not all the physical processes involved in this dependence are yet understood. For this reason, only empirical σ_0 models are available.

The first σ_0 model applied by ESA to ERS-1 data is called CMOD-2 and was tuned by pre-launch air-borne measurements. It was replaced by CMOD-3 on 30 April 92. CMOD-3 is a reformulation of CMOD-2, based on a post-launch tuning using global meteorological model data provided by the European Centre for Medium-Range Weather Forecast (ECMWF). The use of CMOD-3 led to a significant improvement in the determined wind fields (Lecomte and Attema, 1993). The next version of the model, CMOD-4, also based on the ECMWF model data, was activated on 24 February 1993. In addition to the ESA models, CMOD-3 and CMOD-4, we also investigate the model of Wismann (1993) and a model developed at IFREMER (Quilfen, 1992), both based on ERS-1 data. Wismann (1993) tuned his model with wind data obtained from an air-borne scatterometer, buoys and ships in the Norwegian Sea during fall 1991. Quilfen (1992) used wind data from NOAA buoys around the coasts of the USA. Explicit formulas of the four models mentioned are given in Appendix A.

To determine the wind vector, three measurements of σ_0 from different directions are available. A unique solution to this problem requires a correct σ_0 model and data not perturbed by noise, both of which are not available. Cavanie and Lecomte (1987) defined a maximum likelihood function, from which possible solutions are found by searching for local minima. In general, two probable solutions are found, which have about the same speed but nearly opposite direction. No internal rule is efficient at the present time to resolve this upwind/downwind ambiguity (Quilfen, 1992), and external information has to be used for finding the right direction. Stoffelen and Anderson (1993) found that by applying the maximum likelihood function mentioned some directions become very unlikely. They proposed a least-squares function, by which no directions are excluded. The least-squares function is also used in the retrieval algorithm described in Appendix A and applied to the data of this report. Analysed wind fields of the UKMO are used to resolve the directional ambiguity.

3

Measured and analysed winds

Real winds, together with surface meteorological parameters and water temperature, have been measured during three cruises (NORDIC'91, NORDIC'92a and '92b) from on board R/V *Alliance* in the IFF area. This section describes the experiments. Time series of the collected data are presented in Appendix B. In addition to the *in situ* data, analysed winds from the wind archive of the UKMO will be used for comparison with scatterometer-retrieved winds. This chapter contains a comparison of *in situ* and analysed wind velocities.

3.1. WINDS MEASURED FROM ON BOARD R/V ALLIANCE

NORDIC'91 began from Rosyth (Scotland) on 13 August 1991 and ended in Tórshavn (Faeroe Islands) on 30 August 1991 with a port call in Reykjavik (Iceland) on 22/23 August 92. NORDIC'92a consisted of two parts, the first for oceanographic investigations, starting in Greenock (Scotland) on 29 February 1992, ending in Tórshavn on 19 March 92, and the second for mainly acoustic investigations starting on 21 March 92, ending on 28 March 92 in Tórshavn. NORDIC'92b covered the period from 13–29 October 92, starting in Tórshavn and ending in Liverpool.

In situ measurements of surface meteorological data and sea-surface temperature have been performed with the ZENO-*Alliance* network (ZAN), with ZENO and ZAN being trade names of the Coastal Climate Company (Seattle, USA). ZAN is a monitoring system designed especially for shipboard installation, cf. Minnett (1991). The network integrates measurements of apparent wind, air temperature, relative humidity, barometric pressure and water temperature with information on ship location, course and heading. Also downwelling short- and long-wave radiation are measured, but not referred to in the investigations presented here. Wind monitor, temperature and relative humidity sensors are combined into a single module. For providing redundancy, two identical modules are mounted on the foremast at a height of about 16 m above the water line, another one is mounted at the stern of the ship about 12 m above the water. Barometric pressure is recorded at the stern mast, and water temperature is measured at about 2 m below sea level on the port side of R/V *Alliance* (2.5 m above keel). More information on the instrumentation is given in Appendix B.

The data were recorded with 5 min sampling and are presented in Appendix B as time series of 6 days' duration. Displayed are the atmospheric pressure, relative humidity, air and water temperature as well as their difference (Figs. B2a, B3a, B5a,

B6a, B7a, B8a, B10a, B11a). Real winds, as determined from the ship measurements and corrected by the ship's velocity, are presented as 5 min samples and as hourly means (Figs. B2b, B3b, B5b, B6b, B7b, B8b, B10b, B11b). By making use of Eqs. (9, 10), the wind speeds have been adjusted to neutral stability and the reference height of 10 m. In total, data from eight 6-day periods are available. Appendix B also contains the ship tracks during the three cruises (Figs. B1, B4, B9).

3.2. ANALYSED WINDS OF THE UK METEOROLOGICAL OFFICE

Wind data, as required for oceanographic modelling, have to contain both spatial and temporal variability. Such data, on a regular grid with constant time increments, are available from standard weather analysis. The data used in this report are from the assimilated wind archive of the UKMO, which is produced as part of a global data analysis scheme. The analysis is based on a numerical prediction model using primitive equations. It is on a latitude-longitude grid and has 20 vertical levels. Data assimilation is achieved by the repeated insertion of observational increments. Winds are determined at hourly intervals on a grid with a resolution of 0.833° in latitude and 1.25° in longitude. For the purposes of our analysis, winds are taken from the lowest level of the atmospheric model, being roughly 25 m above sea level.

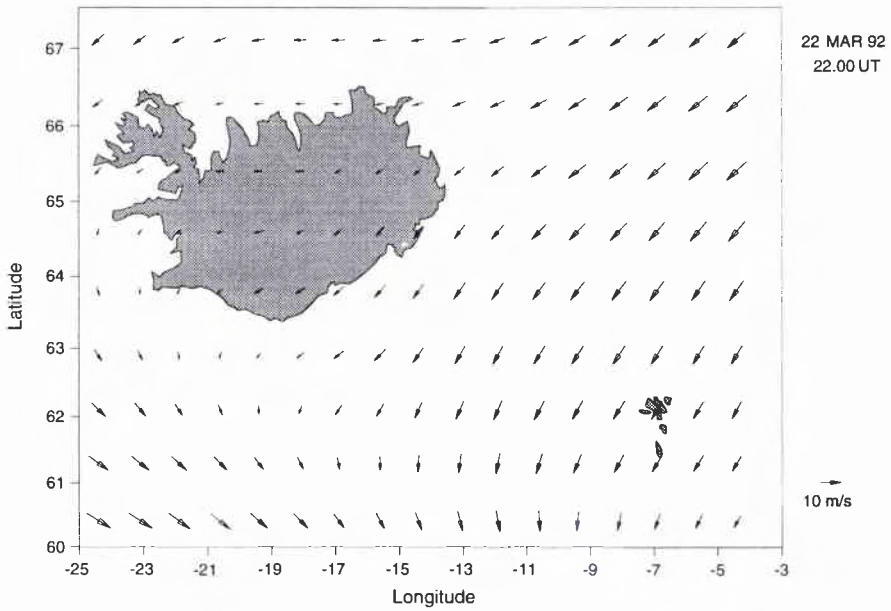

Figure 2 *Wind-field from the standard weather analysis of the UKMO, adjusted to 10 m above sea level (assuming a stable boundary layer). Oceanographic convention is used, i.e. vectors are indicating the direction towards which the wind is blowing.*

Figure 2 presents an example of the wind field as determined by the weather analysis of the UKMO and adjusted to the reference height of 10 m using Eq.(11), i.e. assuming neutral stratification. The length of the vectors is proportional to the wind speed and the arrows are pointing in the direction the wind is blowing (oceanographic convention).

3.3. COMPARISON OF IN SITU AND ANALYSED WINDS

For comparing the analysed with the *in situ* measured winds, the data have to be interpolated from the regular grid to the current position of the ship. This is done by

$$\mathbf{u} = \sum_i g_i \mathbf{u}_i \quad \text{with} \quad g_i = \frac{(R - d_i)^2}{\sum_i (R - d_i)^2}, \tag{12}$$

where $\mathbf{u}$ is the interpolated wind velocity and $\mathbf{u}_i$ are the wind vectors at grid points within a circle of radius R = 100 km around the ship's position, d_i are the distances from the ship to the respective grid points.

Stick-plot time series of the interpolated analysed winds, which are adjusted to neutral stability and 10 m reference height, are presented in Appendix B together with the 1 h means of observed winds (Figs. B2b, B3b, B5b, B6b, B7b, B8b, B10b, B11b). Discarding the data when R/V *Alliance* anchored in an Icelandic fjord (Fig. B5b: 90–124 h, Fig. B10b: 48–80 h), these wind velocities are compared in Fig. 3, separately for the three cruises. The upper panel shows the 1 h means of wind speed. For the respective wind directions (lower panel) only wind vectors with speeds exceeding 5 ms^{-1} have been considered.

The relationship of variables, as compared in Fig. 3, may be quantified by linear regression analysis. An accurate estimation of the regression coefficient requires some knowledge of the error statistic of the variables under investigation (cf. Freilich, 1986), which is not available. In addition, it is questionable whether the considered relationships are linear. For these reasons, we do not estimate the slope of the regression but equate it to its ideal value one,

$$y = x + b, \tag{13}$$

where y represents wind-speed or -direction as measured on board R/V *Alliance* and x the respective value of the analysed winds. This representation is chosen to allow for better comparison with later figures.

For the purpose of estimating the bias and standard deviation the simplified approach Eq. (13) seems to be reasonable. By minimizing the expression,

$$\epsilon^2 = \sum_i (y_i - x_i - b)^2, \tag{14}$$

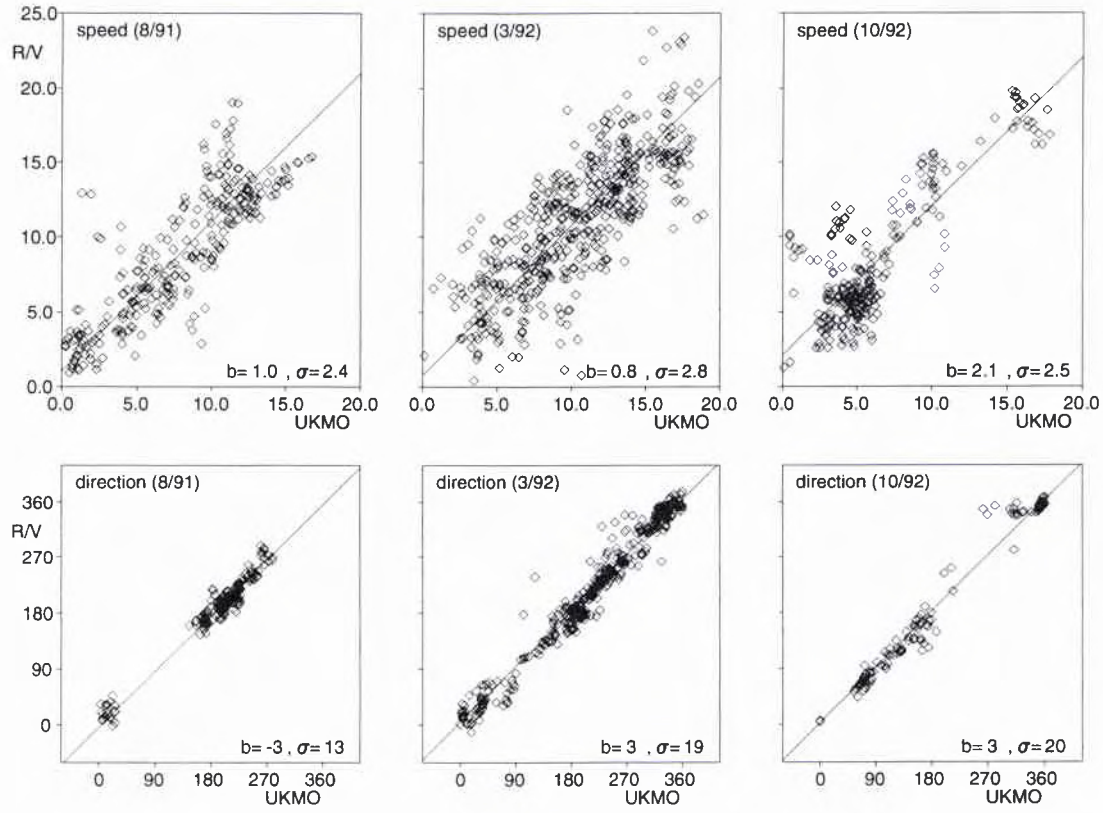

Figure 3 *Comparison of wind speeds and directions, as measured on board R/V Alliance, and interpolated to ship's position from the analysed wind fields of the UKMO. Wind speeds are adjusted to neutral stratification and 10 m height. Wind directions are compared only if both speeds exceed 5 ms^{-1}. The data are from three cruises: NORDIC'91, NORDIC'92a and '92b.*

with the summation extending over all pairs of variables (y_i, x_i) available, the bias b and the variance $\sigma^2 = \epsilon^2/(N-1)$ become,

$$b = \frac{1}{N}\sum_i (y_i - x_i), \qquad \sigma^2 = \frac{1}{N-1}[\sum_i (y_i - x_i)^2 - Nb^2]. \tag{15}$$

Figure 3 shows a relatively high scatter of wind speeds with standard deviations σ of the order of 2.5 ms^{-1} for all three cruises. The bias is about 1.0 ms^{-1} for the first two experiments and 2.0 ms^{-1} for the last one. In all cases the mean measured wind speed exceeds the analysed one. The directions show only a small bias of $\pm 3°$, the standard deviation is about 20° for all three experiments. It should be mentioned that the adjustment to neutral stability mainly affects low wind speeds and has nearly no influence on bias and standard deviation in Fig. 3.

A comparison of the time series in Appendix B shows that some of the deviations between observed and analysed winds is due to a higher temporal variability of the real winds, which is smoothed out in the analysed data. In order to eliminate this

Table 1 *Bias b and standard deviation σ of 10 h running means of winds measured on R/V Alliance as compared with the UKMO analysed winds*

Cruise	Speed		Direction	
month/year	b [ms^{-1}]	σ [ms^{-1}]	b [deg]	σ [deg]
8/91	0.5	1.9	−4	15
3/92	−0.1	2.4	4	20
10/92	1.4	2.2	0	16

effect, the above analysis has been repeated with 10 h running means of the *in situ* wind vectors. The agreement between measured and analysed winds increases slightly. Biases b and standard deviations σ, computed as for Fig. 3, are presented in Table 1. For the speeds, the biases decrease considerably, but the standard deviations by only about 15%. Little changes occur for the wind directions.

As a result it may be stated that by comparing measured and analysed wind speeds the standard deviation is about 2.5 ms^{-1}. This fact should be taken into account when comparing satellite-retrieved and analysed winds. Though wind observations from on board R/V *Alliance* have been assimilated in the analysed winds, some strong deviations in speed are obvious in all the Figs. B2b, B3b, B5b, B6b, B7b, B8b, B10b, B11b.

Analysed wind data are not only used to tune σ_0 models but also to overcome the ambiguity problem of these models (cf. Subsect. 2.4). For this purpose it is worthwhile to investigate the absolute difference between the measured and analysed wind directions. If this value exceeds 90°, the algorithm described in Appendix A will find a wrong wind direction. With the constraint on wind speeds as used in Fig. 3 this happens in 2 cases (out of 690), but in 20 cases (out of 988) without the constraint.

4

Comparison of scatterometer and other wind data

When comparing *in situ* measured winds with those retrieved from SCAT, it has to be taken into account that both represent different quantities, the first refer to isolated points while the latter are averages over an area of 50 km in diameter. If the wind field is homogeneous and stationary, time averages taken from the *in situ* data may be compared with the spatial averages. The averaging time necessary is determined by the mean wind velocity. A mean velocity of 10 ms^{-1} corresponds to a distance of 36 km per hour. Thus, the averaging time should be at least 1 h. The wind field can assumed to be stationary if the mean wind vector does not change considerably within a few hours. Assuming that the mean wind is advecting the superimposed fluctuations then the field is also homogeneous.

Figure 4 shows a SCAT swath over the IFF area. The arrows represent wind velocities as retrieved by ESA (using the prelaunch CMOD-2 model). Wind velocities have not been determined for grid points marked by a diamond, for which all three cross sections are available, and for those marked by a point, with less than three cross sections available. The analysed wind field for the time of the satellite overpass is shown in Fig. 2.

Figure 5 refers to the section marked in Fig. 4. Wind velocities are displayed as obtained with different σ_0 models (dense vector field). The SCAT-retrieved winds correspond to an equivalent neutral stability wind field, referenced to a height of 10 m. Bold vectors in Fig. 5 on the regular grid represent the analysed winds. The vector surrounded by a circle is the wind measured from on board R/V *Alliance*, averaged over 1 h. The analysed and measured wind speeds are adjusted to the reference height of 10 m by means of Eq. (11), assuming a neutrally stratified atmospheric boundary layer. They are not corrected for stability because for most of the scenes investigated no *in situ* information on the air/sea temperature difference is available.

For the cruise NORDIC'91, correctly calibrated SCAT data are not yet available, and for the cruises NORDIC'92a and '92b only 10 coincident wind data from board R/V *Alliance* and the SCAT have been found. Table 2 contains the wind data (speed and direction) from R/V *Alliance* (1 h means), from the analysed wind field (closest grid point) and retrieved from the SCAT data by applying different σ_0 models. The *in situ* and analysed wind speeds are adjusted to neutral stability and 10 m height by means of Eq. (9, 10).

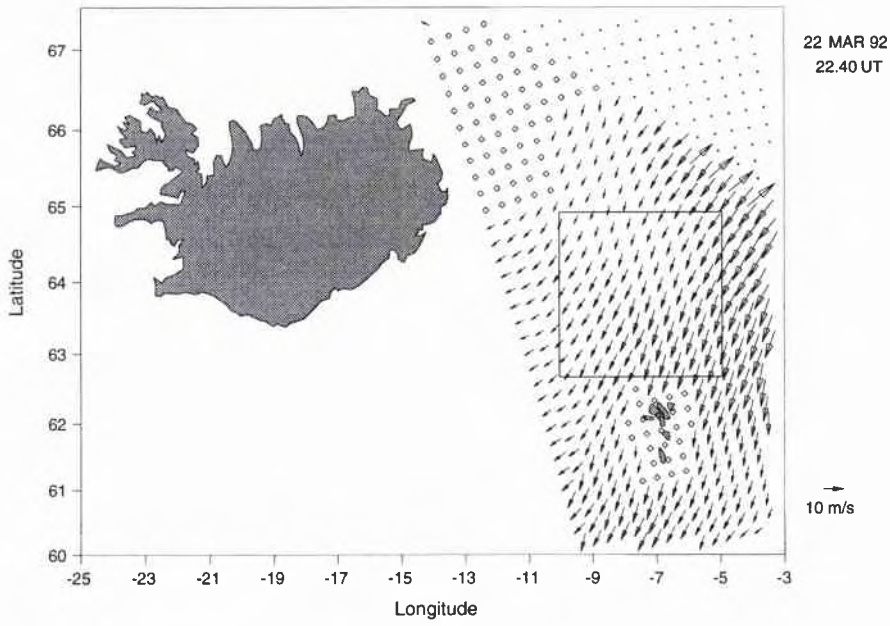

Figure 4 *SCAT swath of ERS-1 in the Iceland–Faeroe area. The arrows represent wind vectors (retrieved with the CMOD-2 model). The marked section is referred to in Fig. 5.*

On 7 March 92 (NORDIC'92a) both measured and analysed wind speed are considerably higher than those retrieved from the SCAT. The IFREMER model yields the highest value, which is still more than 5 ms^{-1} below the measured one. Fig. B6b shows that the wind speed increased during the day reaching 15 ms^{-1} 2 h before the satellite overpass. The position of R/V *Alliance* was 45 km north of the closest SCAT grid point containing three σ_0 (which are not available further north due to SAR operation). From the winds as measured on R/V *Alliance* it seems unlikely that this difference in position can explain the discrepancy in wind speed. As during the satellite overpass snow was falling, this may have influenced the measurements of σ_0.

The two other high-wind speed situations from NORDIC'92a, 10 March 92 and 22 March 92, in Table 2 show good agreement between measured and retrieved speeds. In both cases, CMOD-3 underestimates speed by about 2 ms^{-1}. The deviations in direction are up to 20°. For the two low wind-speed situations, 15 March 92 and 24 March 92, good agreement is found for the speeds, but for the direction only in the case of the higher measured speed of 5.1 ms^{-1}. For the lower speed of 2.5 ms^{-1} the difference is about 90°. At very low wind speeds the direction is usually not well defined and the observed discrepancy not surprising.

On 17 October 92 (NORDIC'92b), the measured wind speed is 8–10 ms^{-1} higher than that retrieved by the four σ_0 models. R/V *Alliance* steamed about 50 km off the coast of Iceland. The retrieved winds at this position fit well into the overall

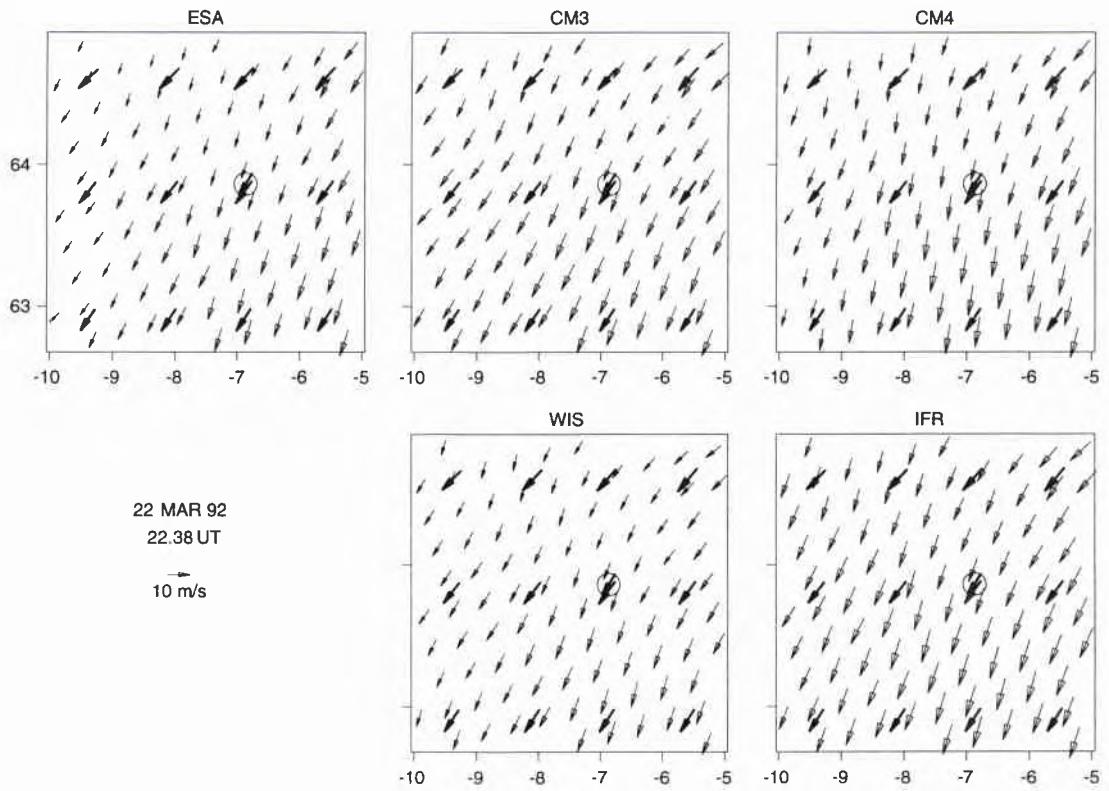

Figure 5 *Wind-field as determined by different σ_0 models: ESA – CMOD-2 (in March 92), CM3 – CMOD-3, CM4 – CMOD-4, WIS – Wismann, IFR – IFREMER. The bold vectors represent analysed winds (on the regular grid), and measured on board Alliance (surrounded by a circle), adjusted to 10 m height by means of (2.10).*

field, and there is no indication of contamination from land. Fig. B10b shows that about 1 h after the satellite overpass a wind front reached R/V *Alliance*, with speeds decreasing to about half their magnitude and direction changing by about 45°. But it is most unlikely that these later winds could have influenced parts of the SCAT coverage area. In addition, the retrieved wind directions agree with that measured before the front passed. Most probably the σ_0 measurements have been influenced by snow showers, as observed on board R/V *Alliance* during the satellite overpass.

The remaining four measurements from NORDIC'92b in Table 2 again consist of two low-wind situations, 20 October 92 and 23 October 92, and two high-wind situations, 26 October 92 and 27 October 92. For the satellite overpass on 20 October 92, the recorded winds show high temporal variability (cf. Fig. B10b). In such situations the comparison of temporal and spatial means becomes questionable. Indeed, the instantaneous wind sample at the time of the satellite overpass yields a speed of 7 ms^{-1}, which agrees much better with the retrieved wind speeds than the 1 h vector average of Table 2. The other low-wind situation (23 October 92) shows good agreement between measured and retrieved winds, for both speed and direction. For the high-wind situations, about the same conclusions may be drawn as for the re-

Table 2 *Comparison of wind speed (U_s) and direction (φ_s), measured on board Alliance ($s = m$), analysed by the UKMO ($s = a$), and derived from the SCAT data with different algorithms: CMOD-3 ($s = 1$), CMOD-4 ($s = 2$), Wismann ($s = 3$), IFREMER ($s = 4$). The measured and analysed winds are adjusted to neutral stability (using the the air/sea temperature difference $T_a - T_w$) and 10 m above sea level. Each five data points are from March 1992 (left) and October 1992 (right), respectively.*

Day	07	10	15	22	24	17	20	23	26	27
time	22.4	22.4	11.5	22.4	11.5	22.6	22.7	22.8	22.9	22.4
lat(N)	66.0	65.3	64.4	63.9	63.5	64.8	64.5	63.8	64.1	60.1
long(W)	11.1	9.6	9.2	6.9	7.8	13.3	12.0	9.0	12.0	7.9
$T_a - T_w$	3.0	−5.2	−6.7	0.4	−0.3	−4.0	0.1	0.9	−1.1	−0.8
U_m	15.0	15.6	5.1	10.7	2.5	22.1	2.4	4.0	13.0	14.1
φ_m	174	300	323	25	204	2	172	95	66	65
U_a	15.7	17.2	4.1	11.7	3.7	16.2	0.5	2.9	7.9	11.2
φ_a	196	305	264	36	248	357	121	117	82	67
U_1	7.5	13.5	4.0	8.0	3.0	12.0	5.5	4.0	8.5	8.5
φ_1	172	317	298	22	290	353	151	93	74	39
U_2	9.5	15.0	4.5	9.5	3.0	14.0	6.5	4.5	10.0	10.5
φ_2	174	313	308	22	286	355	153	99	72	57
U_3	8.0	16.5	4.5	9.5	2.5	11.0	6.5	4.5	9.0	8.0
φ_3	178	319	328	12	318	351	161	115	70	49
U_4	10.0	15.5	5.5	11.0	3.5	13.0	7.5	6.0	12.0	11.5
φ_4	174	319	306	20	298	357	151	105	72	47

spective measurements during NORDIC'92a. CMOD-3 considerably underestimates the measured wind speeds, IFREMER yields the best agreement.

For the following investigations, square sections as in Fig. 5 have been chosen from 30 satellite overpasses during March 92 and October 92 within the area represented by Fig. 2. The side lengths of the sections are 250 km, each covering 12 grid points of the analysed wind field. Winds derived from SCAT have been averaged within a circle of 25 km radius around these grid points, i.e. in total, 360 wind vectors are available for comparison.

Figure 6 compares wind speeds as derived from the SCAT by applying different σ_0 models with analysed wind speeds (upper panel) and with each other (lower panel). The presentation is the same as for Fig. 3. Data are from March 92 (squares) and from October 92 (diamonds). The respective wind directions are compared in Fig. 7. Here, only wind vectors exceeding speeds of 5 ms^{-1} are considered. By comparing SCAT-retrieved against analysed wind speeds and directions (Figs. 6, 7,

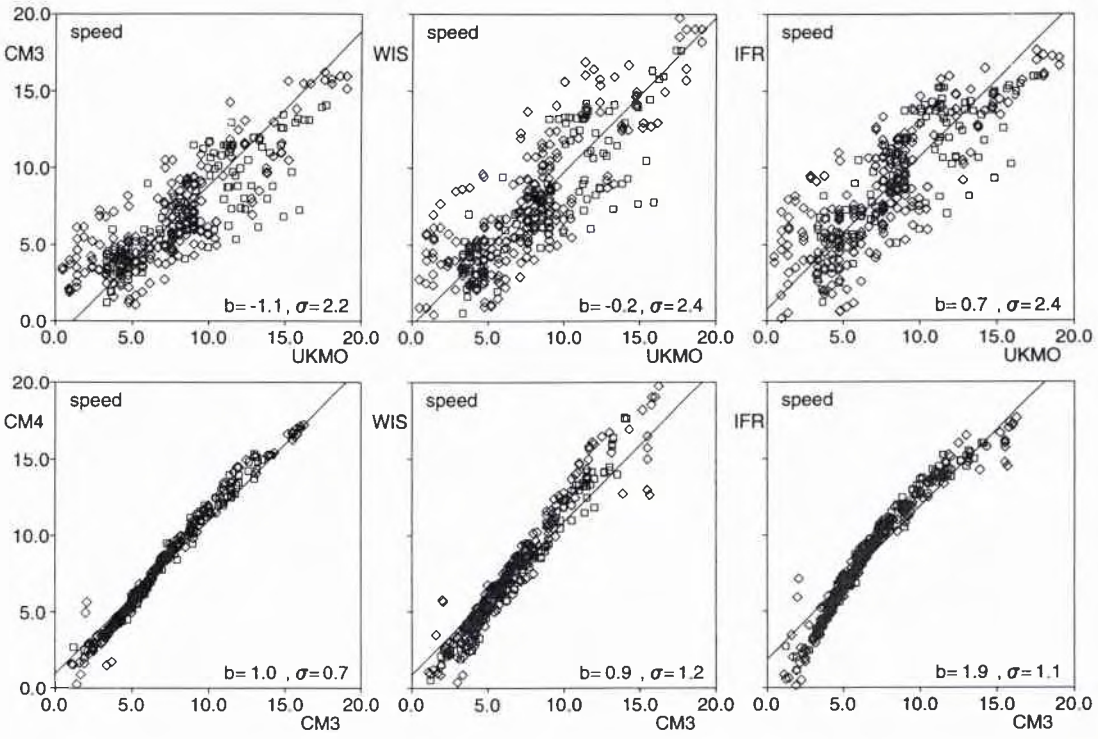

Figure 6 *Comparison of wind speeds, determined from the SCAT by applying different σ_0 models: CM3 – CMOD-3, CM4 – CMOD-4, WIS – Wismann, IFR – IFREMER, with analysed winds of the UKMO and with each other. Data are from March 92 (squares) and October 92 (diamonds). Wind speeds are in ms^{-1}.*

upper panel) it is found that the standard deviations σ, are about the same as for the comparison of measured and analysed winds (cf. Fig. 3). This means that the real performance of the SCAT may be underestimated by using analysed data for comparison. Considerable differences, mainly in the wind speeds, are found between the different σ_0 models (Fig. 6, lower panel). In general, the CMOD-3 retrieved wind speeds are 1–2 ms^{-1} less than those retrieved from the other σ_0 models.

Spatial variability of surface winds is of major importance in driving ocean currents. It is well known that horizontal variations of surface winds may induce vertical motions within the ocean through a mechanism called Ekman pumping. Considering a surface mixed layer of thickness d the vertical velocity w at the base of this layer becomes

$$w(-d) = \frac{1}{\rho_w f} curl_z(\boldsymbol{\tau}), \tag{16}$$

where f is the Coriolis parameter, ρ_w the density of water and $\boldsymbol{\tau}$ the horizontal vector of wind stress. This solution refers to steady conditions and vanishing vertical current velocity at the sea surface. The dependence of wind-stress on wind-velocity is given by (4), which by inserting into (16) yields a dependence of $w(-d)$ on the horizontal derivatives of surface winds. From conventional measurements these deriva-

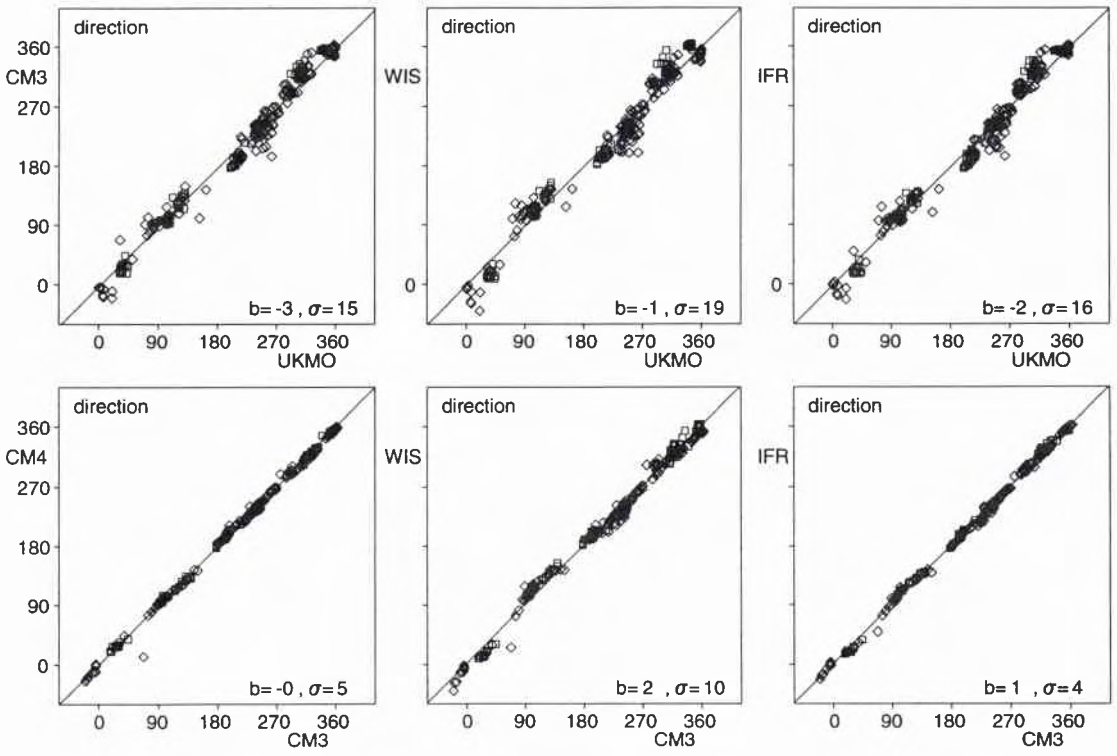

Figure 7 *Comparison of wind directions, determined from the SCAT by applying different σ_0 models: CM3 - CMOD-3, CM4 - CMOD-4, WIS - Wismann, IFR - IFREMER. Only wind vectors with speeds above 5 ms^{-1} are considered. Data are from March 92 (squares) and October 92 (diamonds). Wind directions are in degrees.*

tives are hard to determine but may be easily computed from satellite-retrieved wind fields.

Horizontal derivatives as computed from the satellite-retrieved and analysed wind fields are compared, as are the values obtained by applying different σ_0 models. From the four possible derivatives of a horizontal vector we confine ourselves to the two quantities, horizontal divergence div_{h} and vertical component of curl $curl_z$,

$$div_{\mathrm{h}} = \frac{\partial u}{\partial x} + \frac{\partial v}{\partial y}, \qquad curl_z = \frac{\partial v}{\partial x} - \frac{\partial u}{\partial y}, \tag{17}$$

where (u, v) is the horizontal wind vector with the components u parallel to x (east) and v parallel to y (north). Horizontal derivatives of the wind vector may vary with the scale considered, e.g. considering a sudden change in wind-speed over a front, the numerical value of the across-frontal derivative changes with the distance from which it is computed. The horizontal derivatives from the analysed wind field are computed from central differences with reference to the centre of the areas considered. From the satellite-retrieved winds, horizontal derivatives are determined from data within circles of given diameter by means of least-squares fitting. East

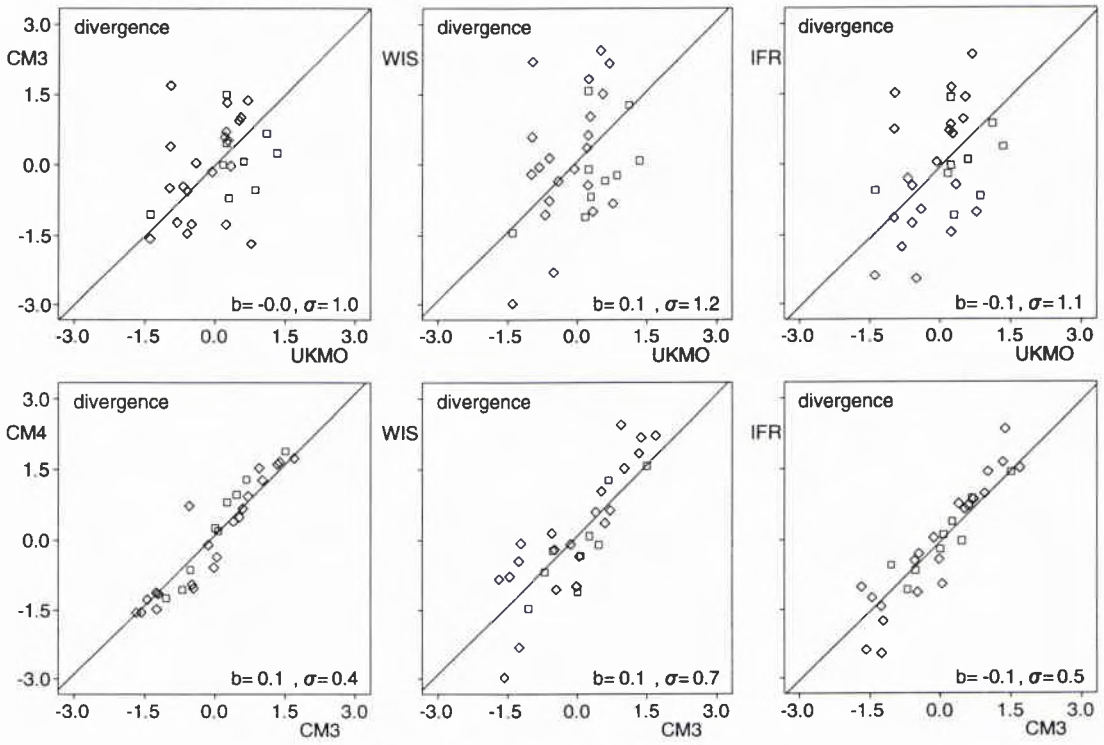

Figure 8 *Comparison of horizontal divergence determined from the SCAT by applying different σ_0 models: CM3 - CMOD-3, CM4 - CMOD-4, WIS - Wismann, IFR - IFREMER with analysed winds of the UKMO and with each other. Data are from March 92 (squares) and October 92 (diamonds). Units are in 10^{-5} s^{-1}.*

and north components of the wind vector (u, v) are approximated by first-order polynomials,

$$u = a_0 + a_1 x + a_2 y, \qquad v = b_0 + b_1 x + b_2 y. \tag{18}$$

The polynomial coefficients a_l and b_l are determined by minimizing the least-squares sum,

$$\epsilon^2 = \sum_{i=1}^{N} [(u_i - a_0 - a_1 x_i - a_2 y_i)^2 + (v_i - b_0 - b_1 x_i - b_2 y_i)^2], \tag{19}$$

where (u_i, v_i) are the N satellite-derived wind vectors at positions (x_i, y_i) falling into the given circle. By defining the circle's centre as the origin of coordinates $(0, 0)$, the coefficients a_l and b_l represent mean velocities $(l = 1)$ and first-order derivatives $(l = 2, 3)$ at this point. In particular, the horizontal divergence and the vertical component of the curl become

$$div_{\mathrm{h}} = a_1 + b_2, \qquad curl_z = b_1 - a_2. \tag{20}$$

Figure 8 (upper panels) compares the horizontal divergence as determined from the analysed wind fields with that computed from satellite-retrieved wind fields.

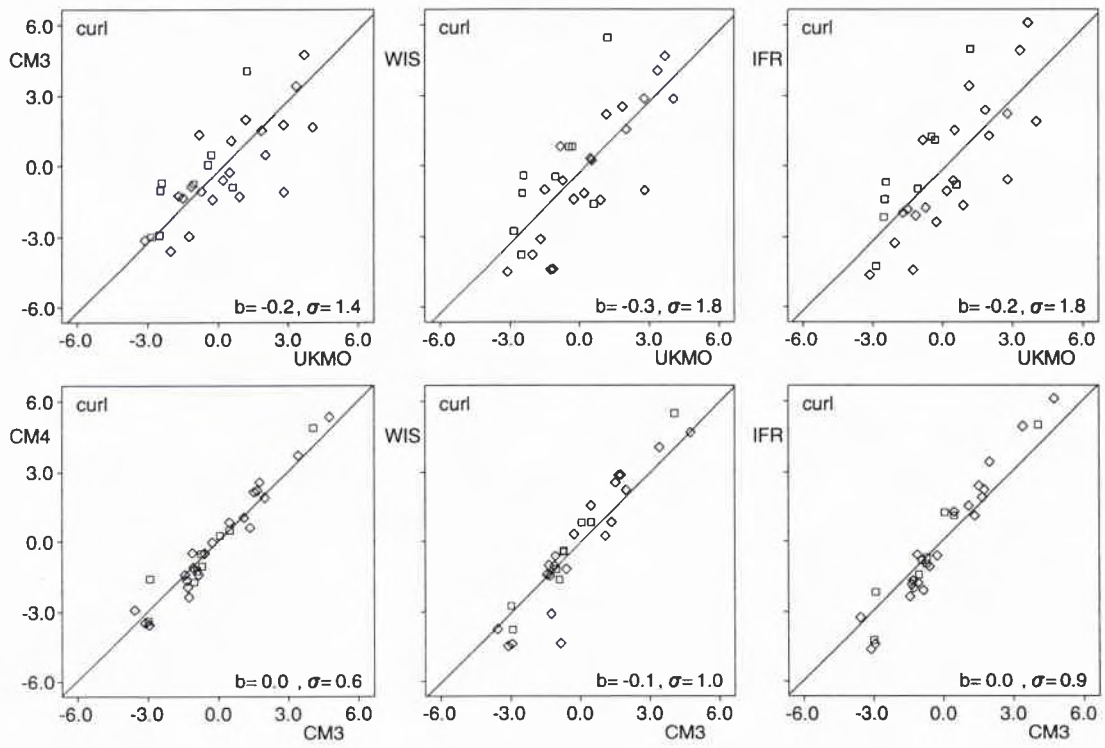

Figure 9 *Comparison of the vertical component of curl, determined from the SCAT by applying different σ_0 models: CM3 - CMOD-3, CM4 - CMOD-4, WIS - Wismann, IFR - IFREMER with analysed winds of the UKMO and with each other. Data are from March 92 (squares) and October 92 (diamonds). Units are in 10^{-5} s^{-1}.*

In accordance with the distance of the central differences of the analysed data a diameter of 250 km has been chosen for the averaging circle. Bias b and standard deviation σ are computed by means of (15). The lower panels of Fig. 8 compare horizontal divergences as obtained with different σ_0 models. Though the divergences as obtained from the analysed data and the SCAT-retrieved winds are of the same order of magnitude there is only little correlation. Divergences from winds retrieved with different σ_0 models show good correlation and nearly no bias.

In Fig. 9 the same investigations as in Fig. 8 are applied to the vertical component of curl. $curl_z$ and div_h are of the same dimension, but the computed numerical values of $curl_z$, both from the analysed and SCAT-retrieved winds, extend over a range twice as large as for div_h. There is also higher correlation between the analysed and SCAT-retrieved curl. Different σ_0 models have about the same influence on curl as on divergence.

Figure 10 investigates the dependence of divergence and curl on the diameter of the averaging circle. The data are from the 30 scences investigated, the first 9 from March 1992 the other 21 from October 1992. Because of similar results we confine ourselves to only one σ_0 model. In the case of wind-fields varying on scales

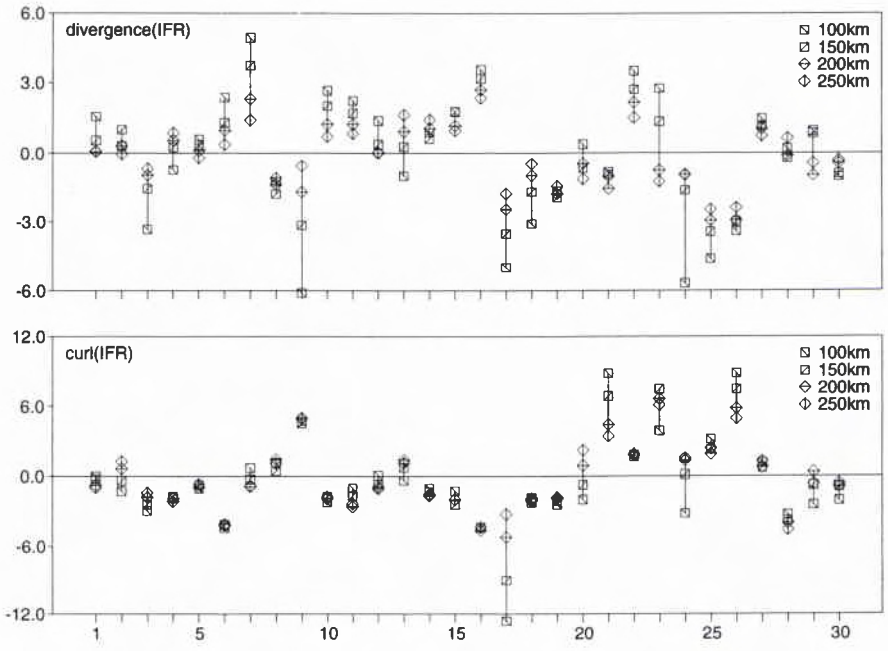

Figure 10 *Horizontal divergence and vertical component of curl, computed with different averaging diameters from SCAT-retrieved winds. For wind-retrieval the IFREMER σ_0 model is used. Units are in $10^{-5}s^{-1}$.*

shorter than 250 km the horizontal derivatives should show a dependence on the averaging diameter, with higher numerical values for smaller diameters. In fact, the divergence shows this behaviour for most of the data, while the curl is more stable. The interpretation of this result is difficult. Noise may be of influence, but it seems that the divergence varies on smaller scales than the curl. An exception is the scene with the highest changes in curl (no. 17), which is from 13 October 1992 and displayed in Fig. A2.

5
Conclusions

Only a limited sample of ten coincident *in situ* and satellite-retrieved wind vectors is available for comparison, which does not allow general conclusions to be drawn. For most of the data, agreement is good, but two cases have been found where the real winds (15 ms^{-1} and 22 ms^{-1}) are considerably underestimated by all four σ_0 models applied, cf. Table 2. For both satellite overpasses, snowfall was recorded on board R/V *Alliance*. Snow as well as rain may influence the roughness spectrum at the sea surface and thus σ_0. Another, probably more important effect, is the attenuation of radar signals in the intervening atmosphere due to scattering. In the IFF area, snow- or rain-fall is a frequent phenomena, and has to be taken into account by making use of scatterometer-retrieved winds.

More data are available for comparing scatterometer-retrieved and analysed winds of the UKMO. In order to investigate the quality of the analysed data, they have been compared with the *in situ* data from the three cruises. A mean bias of about 1.5 ms^{-1} has been found (Fig. 3), by which the analysed wind speeds are less than the measured ones. The bias decreases to 0.5 ms^{-1} after filtering the measured data by a 10 h running vector mean (Table 1). This behaviour is not surprising (because the analysed data represent a smoothed field), but should be taken into account when tuning σ_0 models with analysed data. Another important result is the high standard deviation of about 2.5 ms^{-1} found by comparing measured and analysed data. Some of the deviation may be due to errors in the measurement or unsuffcient correction for atmospheric stability, but most is obviously due to the limitations in modelling winds.

By comparing the performance of the different σ_0 models with respect to wind speed, the relationships found are obviously nonlinear (Fig. 6, lower panel). Compared with CMOD-3, all other models yield larger speeds, mainly in the high-speed range. This tendency is more distinct for the IFREMER model than for CMOD-4, the former yielding about a 1 ms^{-1} higher bias than the second. This may be explained by the fact that the IFREMER model has been tuned with *in situ* winds, but CMOD-4 with analysed winds, which tend to underestimate the real wind speed, cf. Fig. 3.

Directions of the analysed winds are used to overcome the ambiguity problem of the σ_0 models. If the direction of the analysed wind deviates by more than $\pm 90°$ from that of the real wind, a wrong direction will be found for the retrieved wind. This happens for 0.3% of the data when only wind vectors with a speed exceeding 5 ms^{-1} are considered, but in 2.0% of the cases without this constraint. For higher

wind speeds the directional discrepancies are found in conjunction with sharp fronts which are smoothed out in the analysed data.

The horizontal divergence and the vertical component of curl have been computed from analysed and scatterometer-retrieved wind fields (Figs. 8,9). Though the divergences as obtained from the two sources are of the same order of magnitude there is only little correlation. Higher correlation is obtained for the curl. Divergence and curl are of the same dimension, but the values of curl extend over a range twice as large as that for divergence. A relative good correlation is found between respective values of divergence and curl as derived by means of different σ_0 models.

References

Cavanie, A. and Lecomte, P. (1987). Study of a method to de-alias winds from the ERS-1 data. Final Report ESA Contract 6874/87/GPI.

Charnock,H. (1981). Air-sea interaction. *In*: Warren, B.A. and Wunsch, C., *eds.*, Evolution of Physical Oceanography. Cambridge, MA, MIT Press: pp. 482–503. [IBSN 0-262-23104-2]

Feindt, F., Wismann, V., Alpers, W. and Keller, W.C. (1986). Airborne measurements of the ocean radar cross section at 5.3 GHz as a function of wind speed. *Radio Science*, **21**, 845–856.

Freilich, M.H. (1986). Satellite scatterometer comparison with surface measurements: techniques and SEASAT results. *In*: Proceedings of a Workshop on ERS-1 Wind and Wave Calibration, Schliersee, Germany, 2–6 June, 1986.

Guymer, T.H. (1987). Remote sensing of sea-surface winds. *In*: Vaughan, R.A., *ed.*, Remote Sensing Applications in Meteorology and Climatology. Dordrecht, Kluwer: pp. 3276–357. [ISBN 90-277-2502-0]

Hühnerfuss, H., Alpers, W., Jones, W. L., Lange, P.A. and Richter, K. (1981). The damping of ocean surface waves by a monomolecular film measured by wave staffs and microwave radars. *Journal of Geophysical Research*, **86**: 429–438.

Keller, W.C., Wismann, V. and Alpers, W. (1989). Tower-based measurements of the ocean C-band radar backscattering cross section. *Journal of Geophysical Research*, **94**: 924–930.

Lecomte, P. and Attema, E.P.W. (1993). Calibration and validation of the ERS-1 wind scatterometer. *In*: Proceedings of the First ERS-1 Symposium, Cannes, France, 4–6 November, 1992. Paris, ESA, pp. 19–29. [ISBN 92-9092-278-8]

Minnett, P.J. (1991). Surface measurements made during the Icelandic Current Experiment (ICE 89) from the R/V *Alliance*, SACLANTCEN SM–247. La Spezia, Italy, SACLANT Undersea Research Centre.

Pond, S. and Pickard, G.L. (1983). Introductory Dynamic Oceanography, 2nd edn. Oxford, Pergamon Press. [ISBN 0-08-028729-8]

Quilfen, Y. (1992). Validation and quality of ERS-1 scatterometer wind data. *In*: Proceedings, ERS-1 Geophysical Validation Workshop, Penhors, Bretagne, France, 27–30 April, 1992. Paris, ESA, pp. 107–112.

Smith, S.D. (1988). Coefficients for sea surface wind stress, heat flux and wind profiles as a function of wind speed and temperature. *Journal of Geophysical Research*, **93**, 15467–15472.

Stewart, R.H. (1985). Methods of Satellite Oceanography. Berkeley, CA, University of California Press. [ISBN 0-520-04226-3]

Stoffelen, A. and Anderson, D.L.T. (1993). ERS-1 scatterometer data characteristics and wind retrieval skill. *In*: Proceedings of the First ERS-1 Symposium, Cannes, France, 4–6 November, 1992. Paris, ESA, pp. 41–47. [ISBN 92-9092-278-8]

Wismann, V. (1993). A C-band wind scatterometer model derived from the data obtained during the ERS-1 calibration/validation campaign. *In*: Proceedings of the First ERS-1 Symposium, Cannes, France, 4–6 November, 1992. Paris, ESA, pp. 55–59. [ISBN 92-9092-278-8]

Wright, J.W. (1968). A new model for sea clutter. *IEEE Transactions on Antennas and Propagation*, **16**, 217–223.

intentionally blank page

Appendix A

Wind-retrieval algorithm

Least-squares methods are applied to determine the wind vector from the radar cross section, as measured from different look angles. The cost-function to be minimized is

$$\epsilon = [\sum_{l=1}^{3}(s_{0i} - \sigma_{0i})^2]^{0.5}, \tag{A1}$$

where the sum is taken over the three look angles. s_{0i} and σ_{0i} are the measured and theoretical linear cross sections, respectively. The theoretical cross section σ_0 depends on the wind speed and wind direction, and also on the look and incidence angle of the scatterometer antenna. Instead of Eq. (A1), other cost functions may be used, e.g. replacing the absolute by weighted relative differences, which then yields the maximum likelihood function of Cavanie and Lecomte (1987). This was applied in the ESA software until 17 June 1992. For reasons already discussed in Subsect. 2.4, the cost function Eq. (A1) has been used since then, but with logarithmic cross sections instead of linear ones. For the data analysed in this report, the choice of linear or logarithmic cross sections in Eq. (A1) has no significant influence on the retrieved wind vectors.

Different models for the theoretical cross section σ_0 are available. Those referred to in this report are listed below. The parameters used are wind speed U [ms^{-1}], wind direction φ [deg], antenna look direction ϕ [deg], and incidence angle θ [deg].

All angles count clockwise with respect to north, both ϕ and θ from the respective grid point at the sea surface to the satellite. The radar cross section s_0, as well as ϕ and θ are available from the ESA data tapes. The wind vector, as represented by U and φ, is determined by minimizing Eq. (A1). This is done by a simple search algorithm, varying the wind speed by steps of 0.5 ms^{-1} and the wind direction by steps of 3°. Models used for determining the theoretical cross sections are

1. CMOD-3 (used by ESA from 30 April 92 to 23 February 93)

$$\begin{aligned} \sigma_0 &= b_0[1 + b_3 \tanh(b_2)\cos(2(\varphi - \phi))]^{1.6}, \\ b_0 &= 10^{\alpha}[U + \beta + b_1 \cos(\varphi - \phi)]^{\gamma}, \end{aligned} \tag{A2}$$

   where α, β and γ are second-order polynomials of θ, the b_i are linear functions of θ and U and the product of both.

2. CMOD-4 (used by ESA since 24 Feb 93):

$$\sigma_0 = b_0[1 + b_1 \cos(\varphi - \phi) + b_3 \tanh(b_2)\cos(2(\varphi - \phi))]^{1.6},$$

$$b_0 = \delta \times \begin{cases} 10^{\alpha} & \text{if } U+\beta \le 0 \\ 10^{\alpha}(U+\beta)^{\gamma} & \text{if } 0 < U+\beta \le 5 \\ 10^{\alpha+0.3125\gamma\sqrt{U+\beta}} & \text{if } 5 < U+\beta, \end{cases} \tag{A3}$$

where α, β and γ are second-order polynomials of θ. Also δ depends on θ only, and is given as table with 1° resolution. b_1, b_2 and b_3 are linear functions of θ and U and the product of both, with θ-dependent coefficients for b_1.

3. Wismann (1993):

$$\begin{aligned} \sigma_0 &= b_0 + b_1 \cos(\varphi - \phi) + b_2 \cos(2(\varphi - \phi)), \\ b_i &= 10^{\alpha_i} U^{\gamma_i} \qquad (i = 0, 1, 2), \end{aligned} \tag{A4}$$

where α_i and γ_i are second-order polynomials of θ.

4. IFREMER:

$$\begin{aligned} \sigma_0 &= b_0[1 + b_1 \cos(\varphi - \phi) + b_2 \cos(2(\varphi - \phi))], \\ b_0 &= 10^{\alpha+\beta\sqrt{U-\delta}}, \end{aligned} \tag{A5}$$

where α, β and δ are second-order polynomials of θ, b_1 is a linear function of θ and U, b_2 contains linear and quadratic terms in θ and U and the product of both.

Fig. A1 displays the cost function Eq. (A1) in dependence on the wind direction φ for four different wind speeds. The data are from the SCAT of ERS-1, and cost functions are displayed for the algorithm introduced above. It is obvious that the curves contain two main minima about 180°apart. In order to overcome this ambigiuity in determining the wind direction, the analysed wind data of the UKMO are used. The search algorithm only looks for the minimum in the semicircle,

$$\varphi_a - 90° < \varphi < \varphi_a + 90°, \tag{A6}$$

where φ_a is the direction of the analysed wind vector at the closest grid point.

Figure A2 compares wind vectors as supplied by ESA (upper panels) and retrieved by means of the methods described above (lower panels), using the CMOD-3 model. The data presented refer to NORDIC'92b in October 1992, when ESA also applied the CMOD-3 model. Bold vectors represent the analysed winds of the UKMO (adjusted to 10 m height), which are needed to overcome the ambiguity problem by means of Eq. (A6). The first scene from 9 October 1992 shows relatively low winds. The retrieved vectors agree well. Even data discarded by the ESA algorithm yield reasonable winds with our simplified method. The second example from 13 October 1992 displays winds of higher speed and strong horizontal variability. The agreement between both fields is excellent. The third example from 28 October 1992 refers to medium wind speeds. Here the ESA winds change direction by 180° in the lower part of the section displayed. This behaviour is unrealistic and

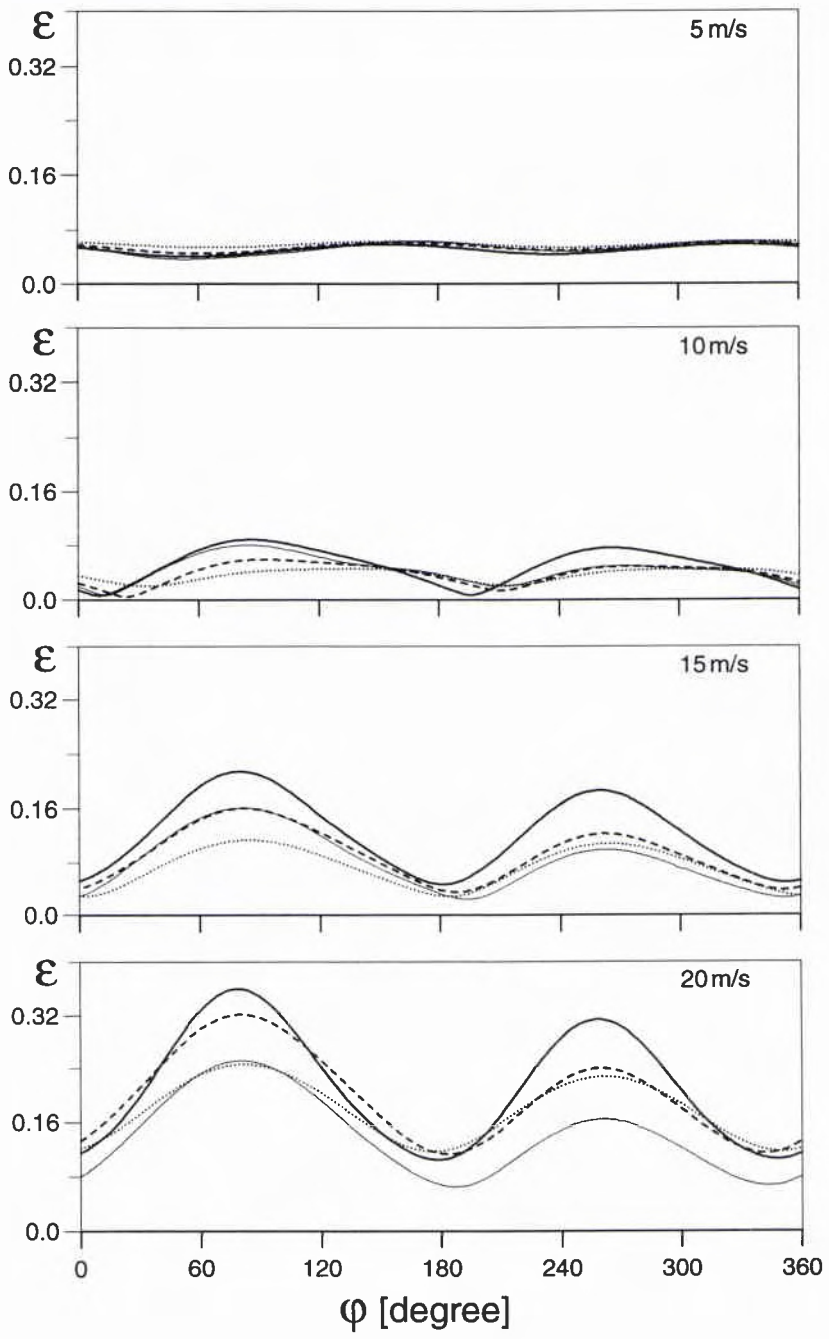

Figure A1 *Dependence of cost function ϵ in (A.1) on wind direction φ for different wind speeds as indicated. SCAT data are from 22 Mar 92, 22:23 UT, 63.74°N, 6.78°W. Curves refer to algorithms: COMD-3 (solid line), CMOD-4 (dashed line), Wismann (thin line), IFREMER (dotted line).*

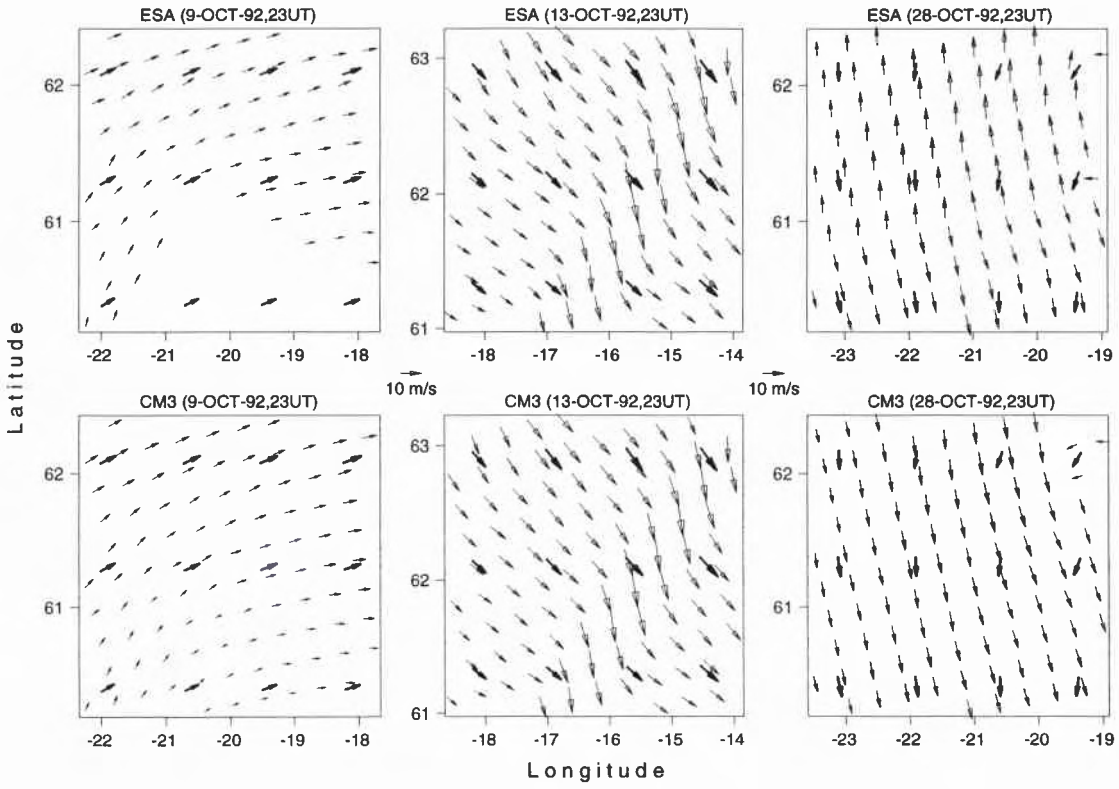

Figure A2 *Comparison of wind vectors retrieved by ESA and by (A1), both using the σ_0 model CMOD-3 (CM3). Three different scenes from NORDIC'92b are presented.*

obviously due to the ambiguity in the σ_0 model. From the 21 scenes analysed for October 1992, 2 contain wind directions differing by about 180° for the two algorithms. In all other cases the wind vectors retrieved by both methods are nearly identical, except for some cases of wind speeds below 5 ms^{-1}.

Appendix B

In situ measurements from on board R/V Alliance

In addition to the description given in Sect. 3, this appendix contains additional information on the measurements from on board R/V *Alliance*, concerning the instrumentation as well as the data collected during NORDIC'91, '92a, and '92b. The variables measured by the ZAN system and referred to in this report are: wind speed and direction, air- and water-temperature, barotropic pressure, and relative humidity.

B.1. INSTRUMENTATION ON R/V ALLIANCE

The wind sensor is an R.M. Young anemometer, originally developed for ocean data buoy use. Wind speed is measured from the rate of rotation of a helicoid shape propeller, and direction by a vane. Each 1 s a sample of wind speed and vane angle is taken and combined to a wind vector relative to the ship. After averaging over a certain time interval, the mean vector is corrected by the ship's velocity as obtained from the Precision Location and Navigation System (PLNS) of R/V *Alliance*. This system provides the ZAN with values of position, ship's true velocity and heading at intervals of about 1 min. Air temperature and relative humidity are measured by a Rotronics hygromer, which combines a precision thermistor and a humidity sensor. The barometric pressure is provided by a Paroscientific pressure sensor, and the water temperature by a Sea-Bird Electronics (SB-3) thermistor.

Sampling of all ZAN instruments during the cruises reported, was performed at 1 Hz and averages over 1 min (i.e. 60 samples) were taken at intervals of 5 min. The times at which the average samples are available is not synchronous for all sensors and different from those of the navigation samples. Before computing real winds and air-sea temperature differences, the various time series were interpolated to a common time base with 5 min spacing by means of linear interpolation.

For the purpose of this report, the most important information comes from the wind anemometers. The accuracy of the instruments is stated to be 0.5 ms^{-1} in speed and 2° in direction. At least for relative accuracy, these values are confirmed by the comparison of the data from both anemometers on the foremast, installed about 1 m apart. Inspection of the instruments at the beginning and end of the cruises gave no evidence of malfunctioning. More important errors than from the instruments may occur from the disturbing influence of the ship's construction. Also the correction for the ship's velocity by means of the PLNS data may introduce errors.

The comparison of the three instruments showed differences in relative humidity up to 5% and differences in air temperature up to 0.5 °C. As often as possible, the measured water temperature was compared with near-surface CTD values. Deviations did not exceed 0.2 °C. Air temperature and water temperature are used to estimate the stability of the atmospheric boundary by their difference. The accuracies mentioned are sufficient for this purpose.

B.2. DATA COLLECTED DURING NORDIC'91, '92A, AND '92B

With respect to oceanography, the aim of the NORDIC project was to collect environmental data in the IFF area, mainly for acoustic purposes. Sound propagation is determined by the sound-speed structure in the ocean, which is controlled by temperature and salinity. Predicting these parameters requires knowledge of the various water masses within the area under investigation, including oceanographic features, such as currents, fronts and eddies. Long-term current monitoring was performed by means of moored current meters, deployed in August 1991 (NORDIC'91) and recovered in March 1992 (NORDIC'92a). Current meters deployed in October 1992 (NORDIC'92b) will be recovered in August 1993. These investigations are supported by satellite-tracked buoys (Argos system). CTD surveys were carried out during all three cruises.

During the two legs of NORDIC'91, surface meteorological data were taken from 15 August 1991 to 20 August 1991, and from 25 August 1991 to 30 August 1991, respectively. Fig. B1 contains the ship's track, the solid line referring to Leg 1 and the dashed line to Leg 2. During Leg 1 a number of current-meter moorings were deployed and a CTD section could be performed. Leg 2 was planned for CTD work only, but bad weather limited the number of stations, and due to ship problems the cruise had to be finished three days before scheduled.

Fig. B2a shows the available time series of pressure, relative humidity, air and water temperature for Leg 1 of NORDIC'91. Multiple curves refer to measurements at different locations on the ship. Due to problems with the automatic recording of the data, water temperatures were lost for a certain period, causing the gap in the time series of water temperature and air-sea temperature difference. The air-sea temperature difference refers to the arithmetic mean of air temperature from the three instruments. The length of the time series is 6 days, i.e. 144 h.

Winds as recorded during Leg 1 by the three instruments on R/V *Alliance* are shown in Fig. B2b. Wind speeds are corrected for neutral stability and to the reference height of 10 m by using the air-water temperature differences of Fig. B2a and applying Eqs. (9,10). North and east component are displayed in oceanographic convention, i.e. a positive east or north component means that the wind is blowing towards this direction. All 5 min samples are displayed for the components. Occasional spikes in the time series result from the imperfect compensation for the ship's motion during rapid manoeuvres, and are hard to remove. In general, the agreement

between the instruments is good. For some periods considerable differences occur, which can be explained by the shadowing effect of the ship's body. The stick plot represents 1 h means computed from the data above by only taking into account the maximum vector at the sample time. In order to suppress the contributions of spikes, wind vectors are discarded if their speed deviates from the mean by more than two times the standard deviation. For comparison, the lowermost panel displays the analysed winds, interpolated to the position of R/V *Alliance* (cf. Sect. 3.3), and also corrected for stability and height.

Fig. B3a presents the same parameters as in Fig. B2a, but for Leg 2 of NORDIC'91. So as to allow better comparison, the time frame is also chosen to be 6 days, though the time series are somewhat shorter. Measured and analysed winds from Leg 2 are displayed in Fig. B3b.

NORDIC'92a consisted of a three-week oceanographic part (Leg 1) and a following one-week acoustic part (Leg 2). Again, 6-day sections of the cruise are considered. The ship's track is shown in Fig. B4. The three 6-day sections of Leg 1 are represented by the solid and dashed line in the left frame and the solid line in the right frame, and Leg 2 by the dashed line in the right frame. In accordance with the presentation of the NORDIC'91 data, Figs. B5a, B6a, B7a, B8a display time series of pressure, humidity and temperature, and Figs. B5b, B6b, B7b, B8b the wind data. During the first week of the cruise the main task was the recovery of moorings. Because of high swell work had to be interrupted for about 36 h with R/V *Alliance* anchoring in an Icelandic fjord. This period becomes clearly visible by the low water temperatures in Fig. B5a.

Also the data of NORDIC'92b are segmented into 6-day periods, the first lasting from 16–21 October 1992, the second from 22–27 October 92. The track of R/V *Alliance* is shown in Fig. B9, the solid lines referring to the first, the dashed line to the second period. Figs. 10a, 10b display time series of pressure, humidity and temperature, and Figs. 10b, 11b the wind data.

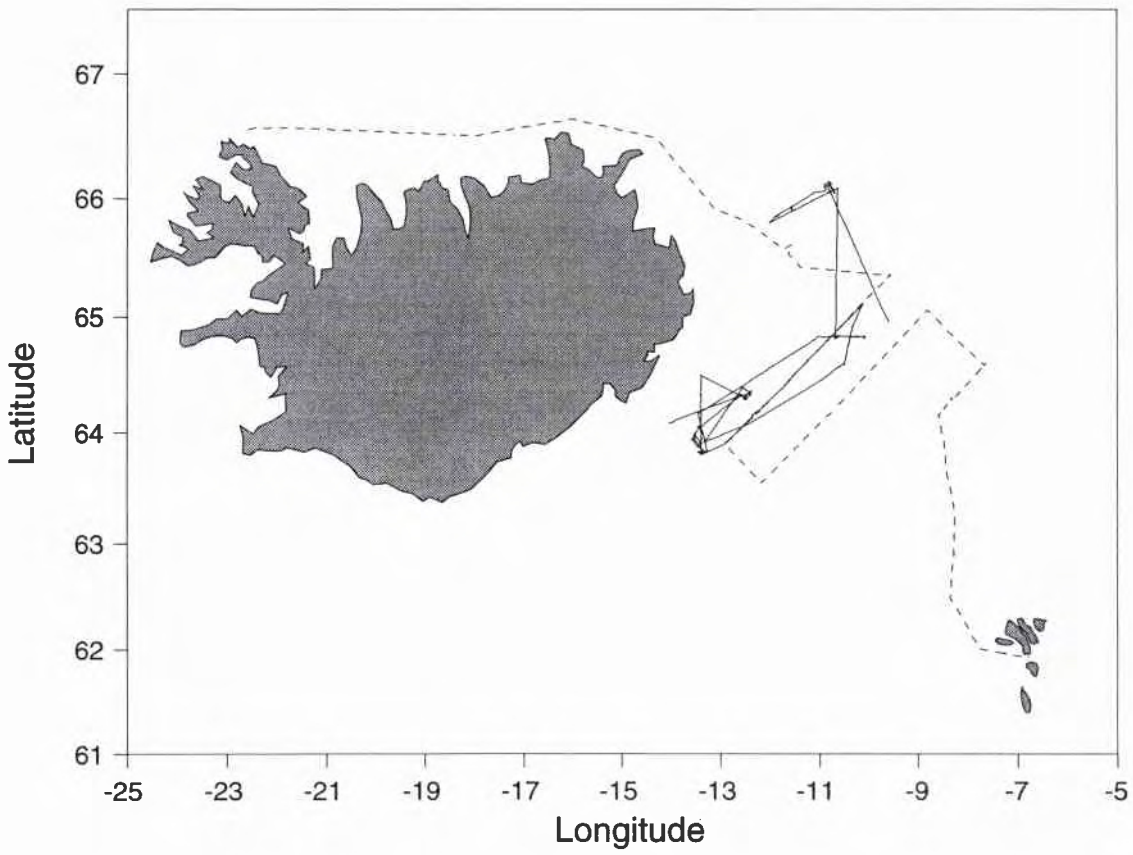

Figure B1 *Track of R/V Alliance during NORDIC'91: Leg 1 (solid line) – from 15 August 1991, 0:00 to 20 August 91, 24:00; Leg 2 (dashed line) – from 25 August 1991, 0:00 to 30 August 1991, 7:00.*

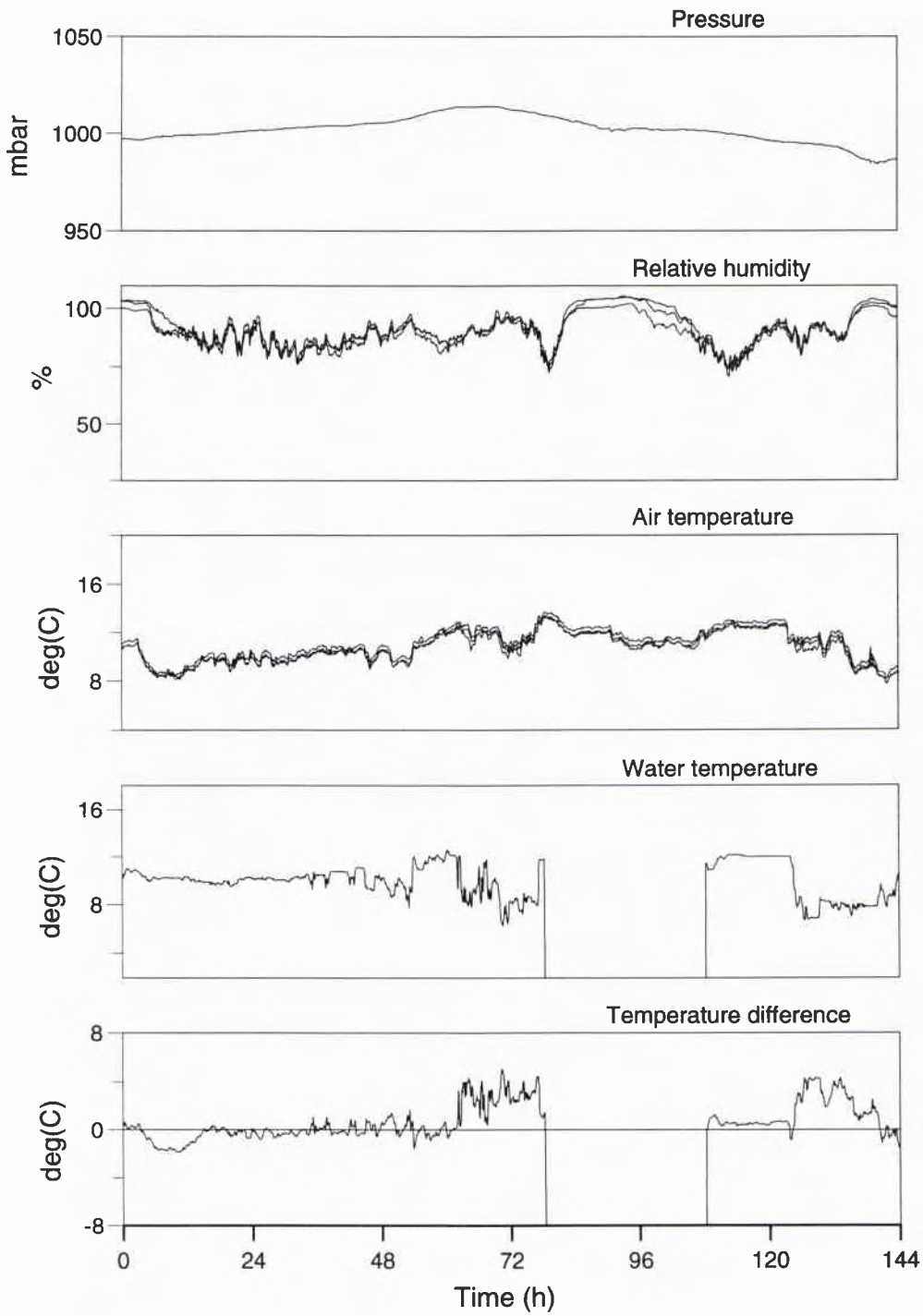

Figure B2a *Surface meteorological data from Leg 1 of NORDIC'91 (15 August 1991), 6-day time series (5min samples), from above: pressure p, relative humidity h (3 sensors), air temperature T_a (3 sensors), water temperature T_w, temperature difference $T_a - T_w$.*

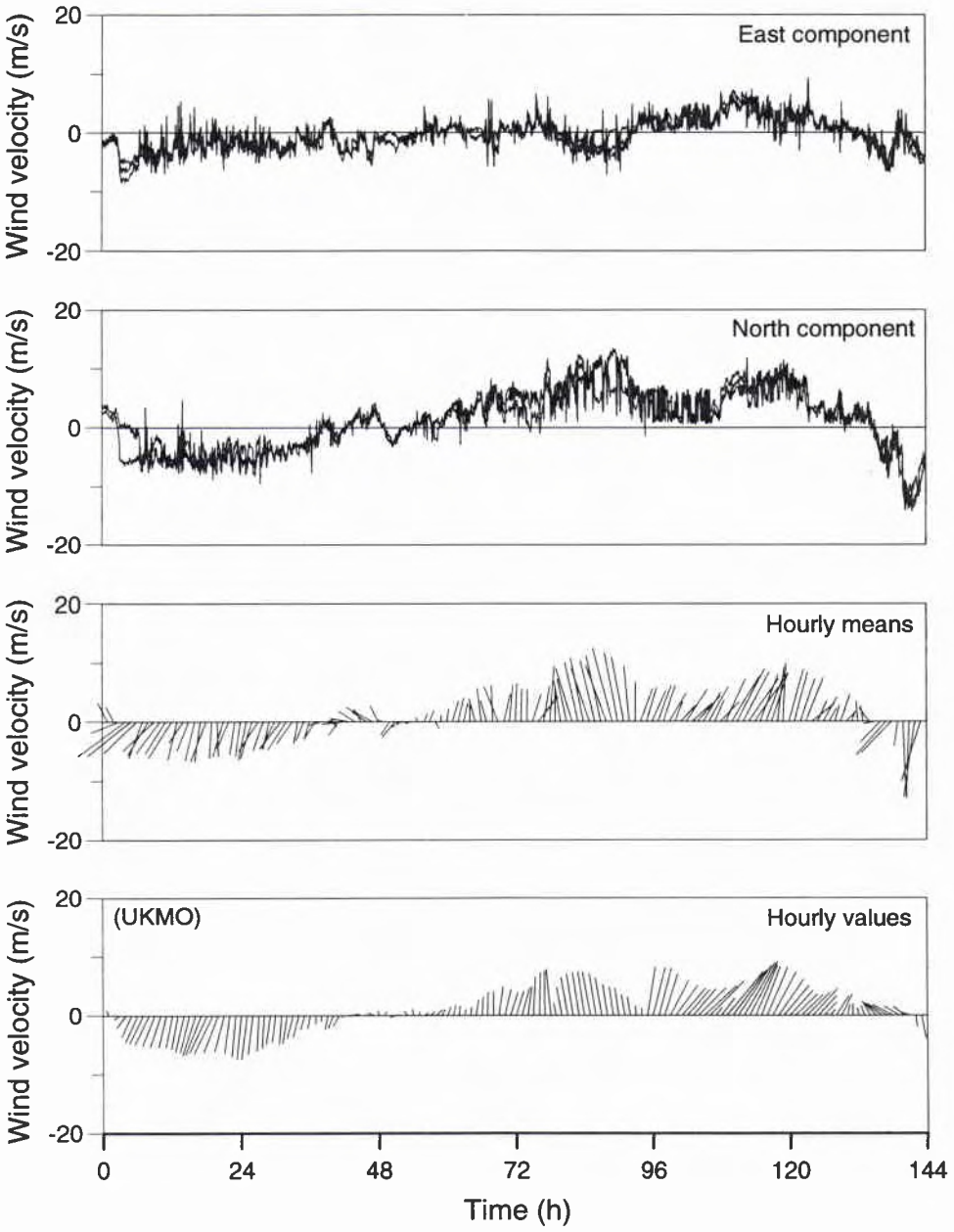

Figure B2b *Measured and analysed winds from Leg 1 of NORDIC'91 (15 August 1991), adjusted to neutral stability and 10 m reference height, 6-day time series, from above: east and north component (3 sensors, 5 min samples), stick plot of 1 h means, and of analysed winds of the UKMO, interpolated to the ship's position. Oceanographic convention is used for displaying the vectors.*

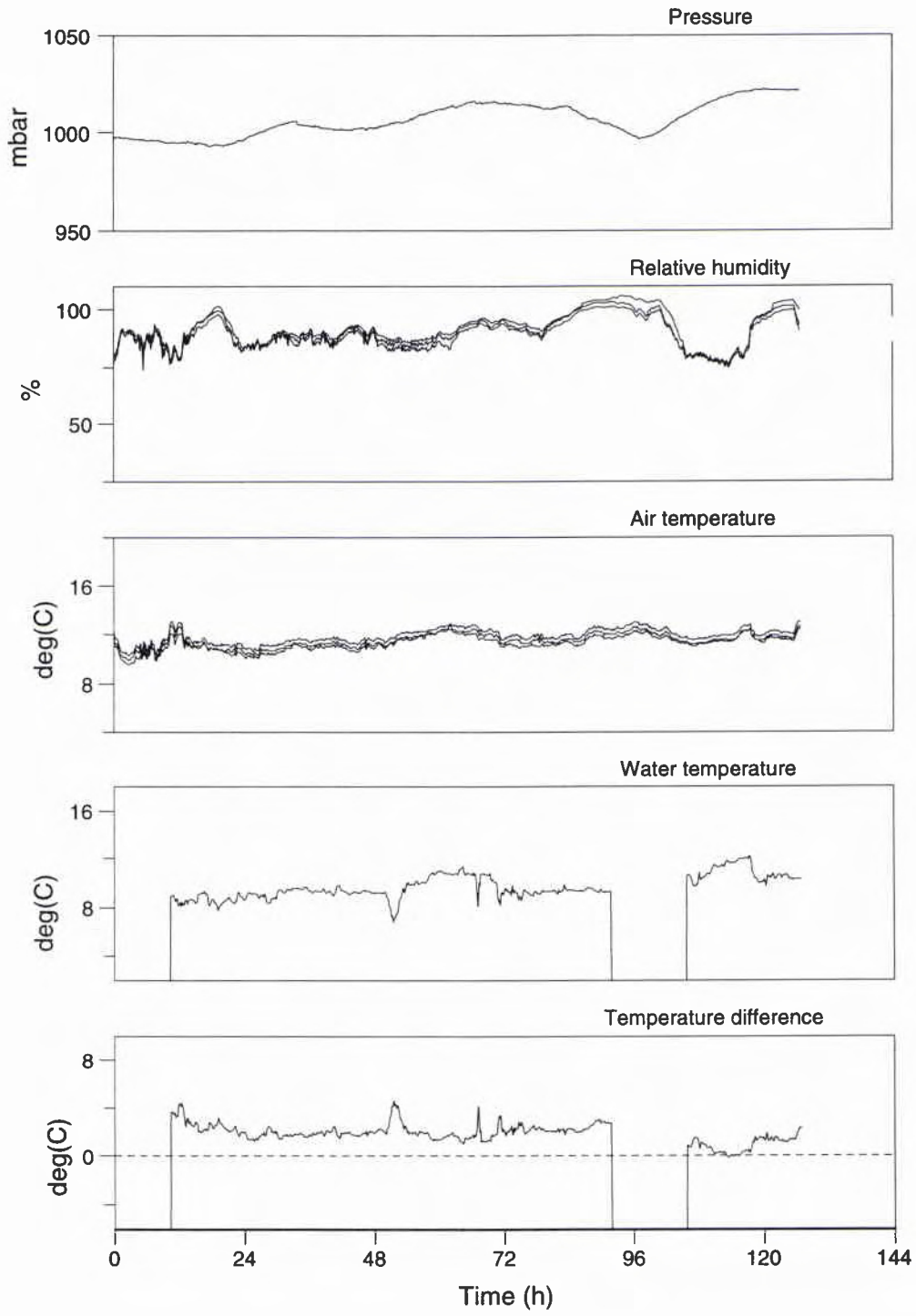

Figure B3a *Surface meteorological data from Leg 2 of NORDIC'91 (25 August 1991), for further explanation cf. Fig. B2a.*

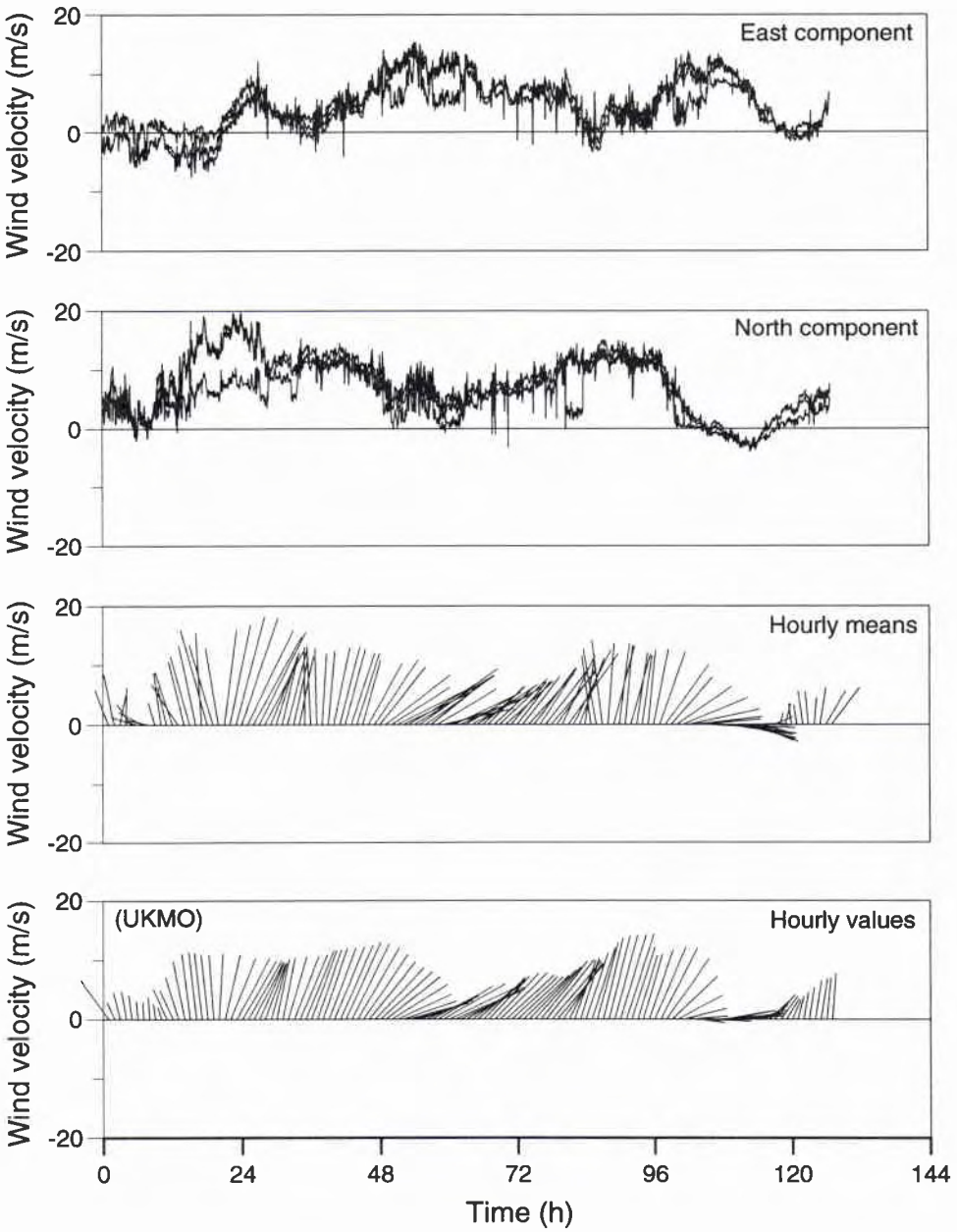

Figure B3b *Measured and analysed winds from Leg 2 of NORDIC'91 (25 August 1991), for further explanation cf. Fig. B2b.*

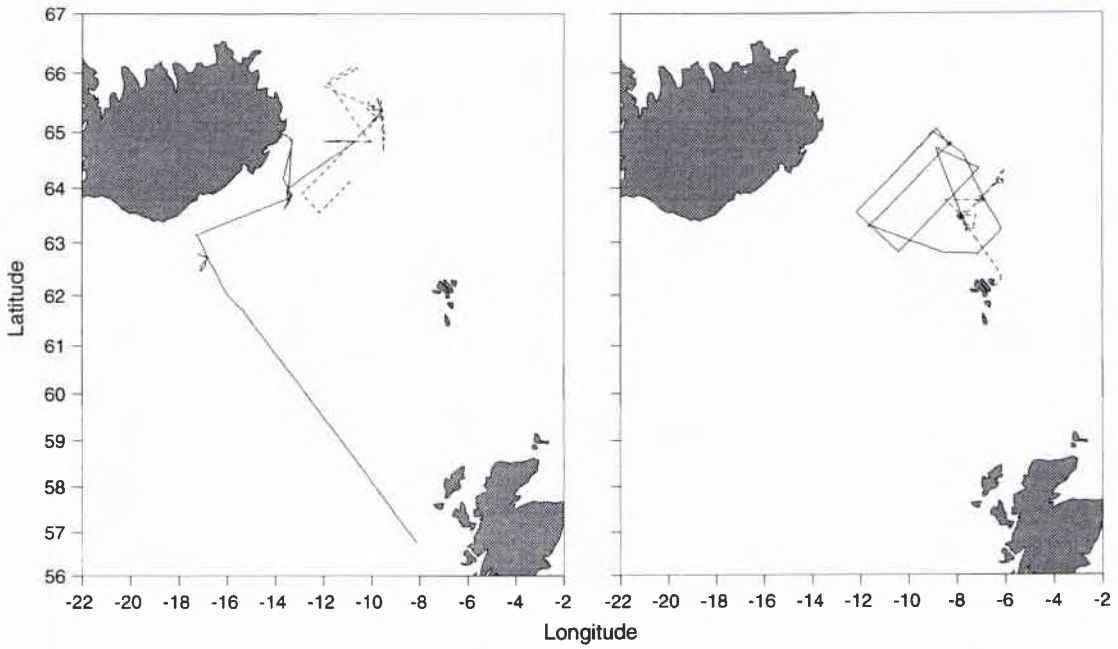

Figure B4 *Track of R/V Alliance during NORDIC'92a: Leg 1a (left, solid line) – from 1 March 1992, 0:00 to 6 March 1992, 24:00; Leg 1b (left, dashed line) – from 7 March 1992, 0:00 to 12 March 1992, 24:00; Leg 1c (right, solid line) – from 13 March 1992, 0:00 to 17 March 1992, 24:00; Leg 2 (right, dashed line) – from 24 March 1992, 0:00 to 30 March 1992, 12:00.*

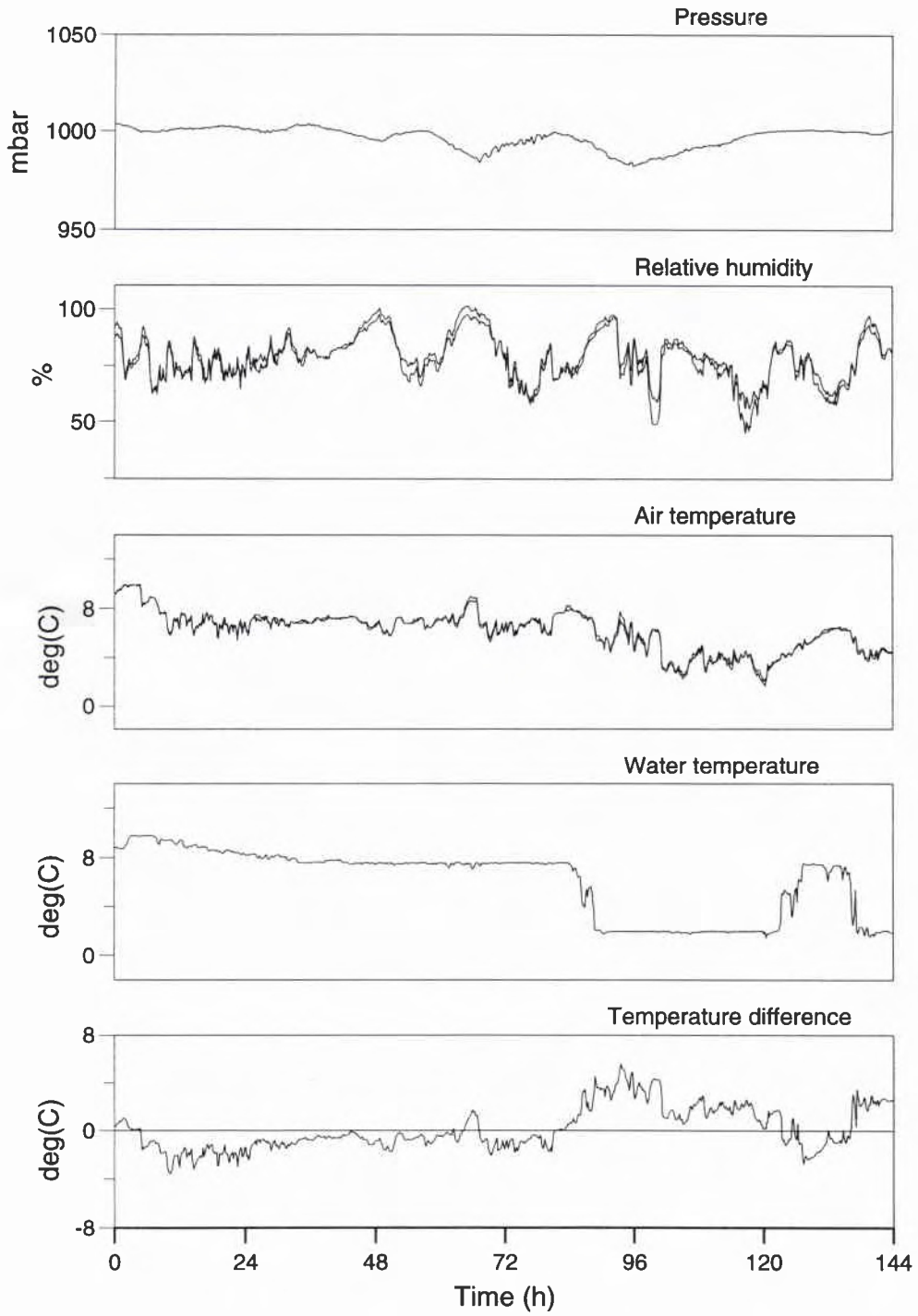

Figure B5a *Surface meteorological data from Leg 1a of NORDIC'92a (1 March 1992), for further explanation cf. Fig. B2a.*

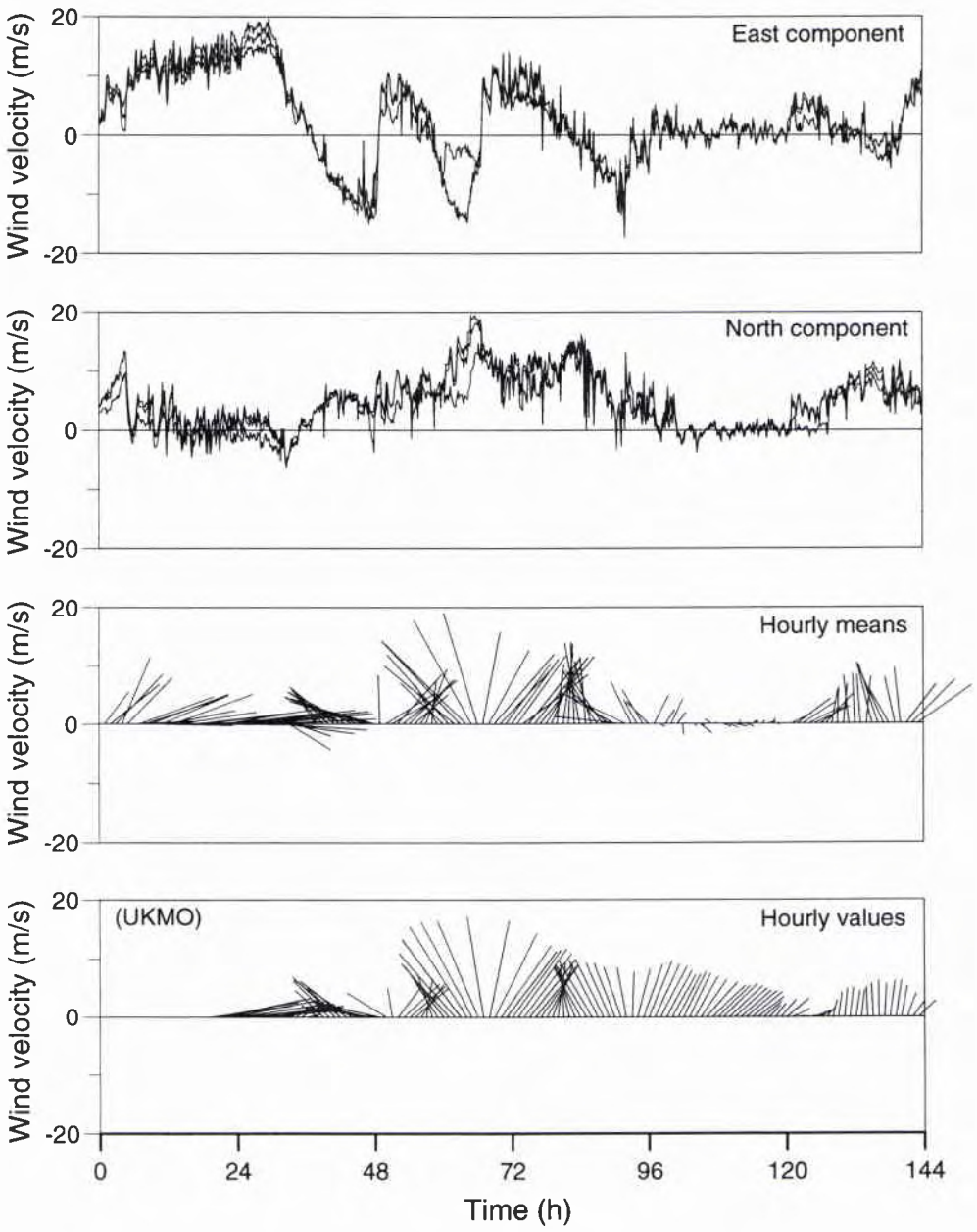

Figure B5b *Measured and analysed winds from Leg 1a of NORDIC'92a (1 March 1992), for further explanation cf. Fig. B2b.*

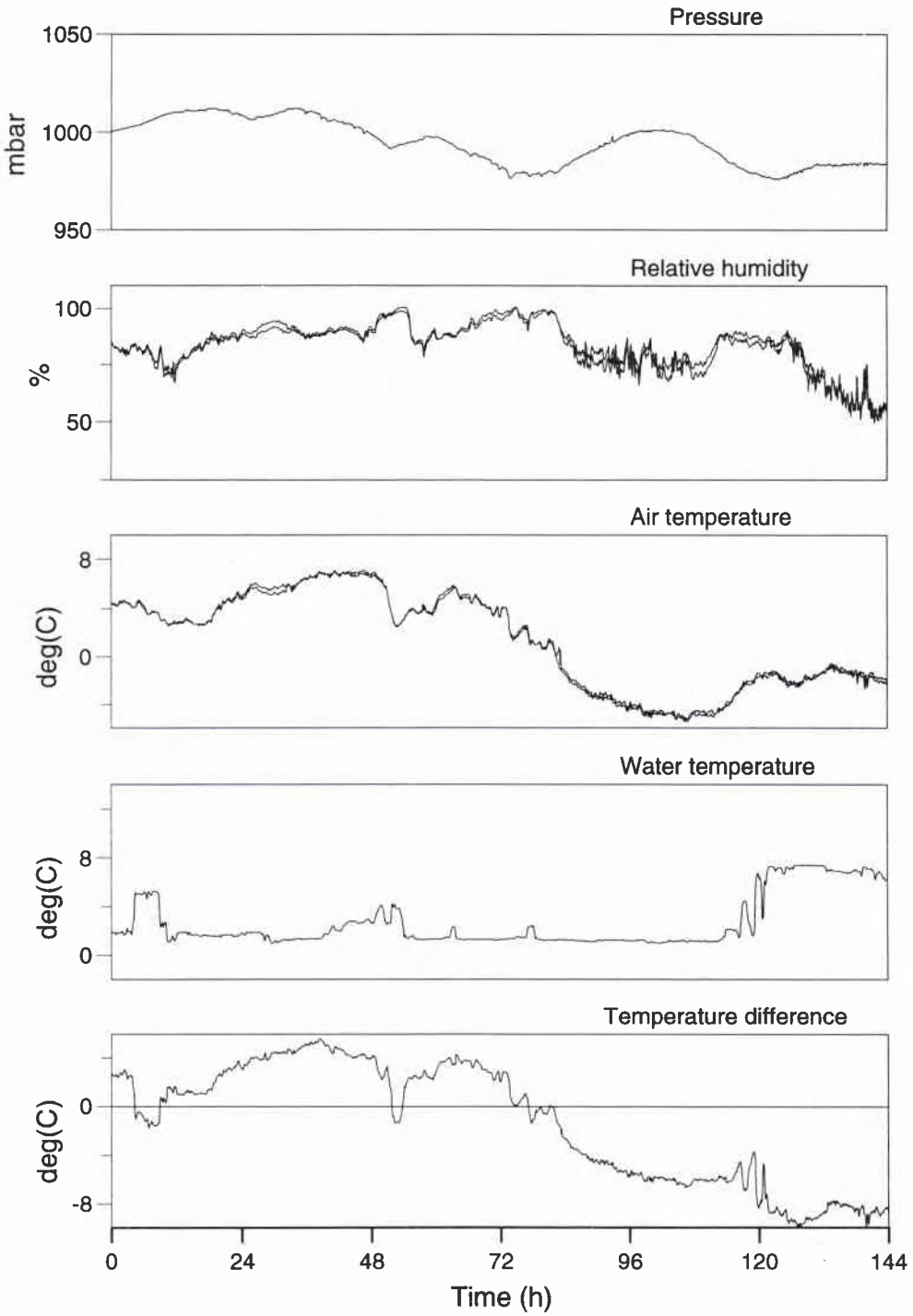

Figure B6a *Surface meteorological data from Leg 1b of NORDIC'92a (7 March 1992), for further explanation cf. Fig. B2a.*

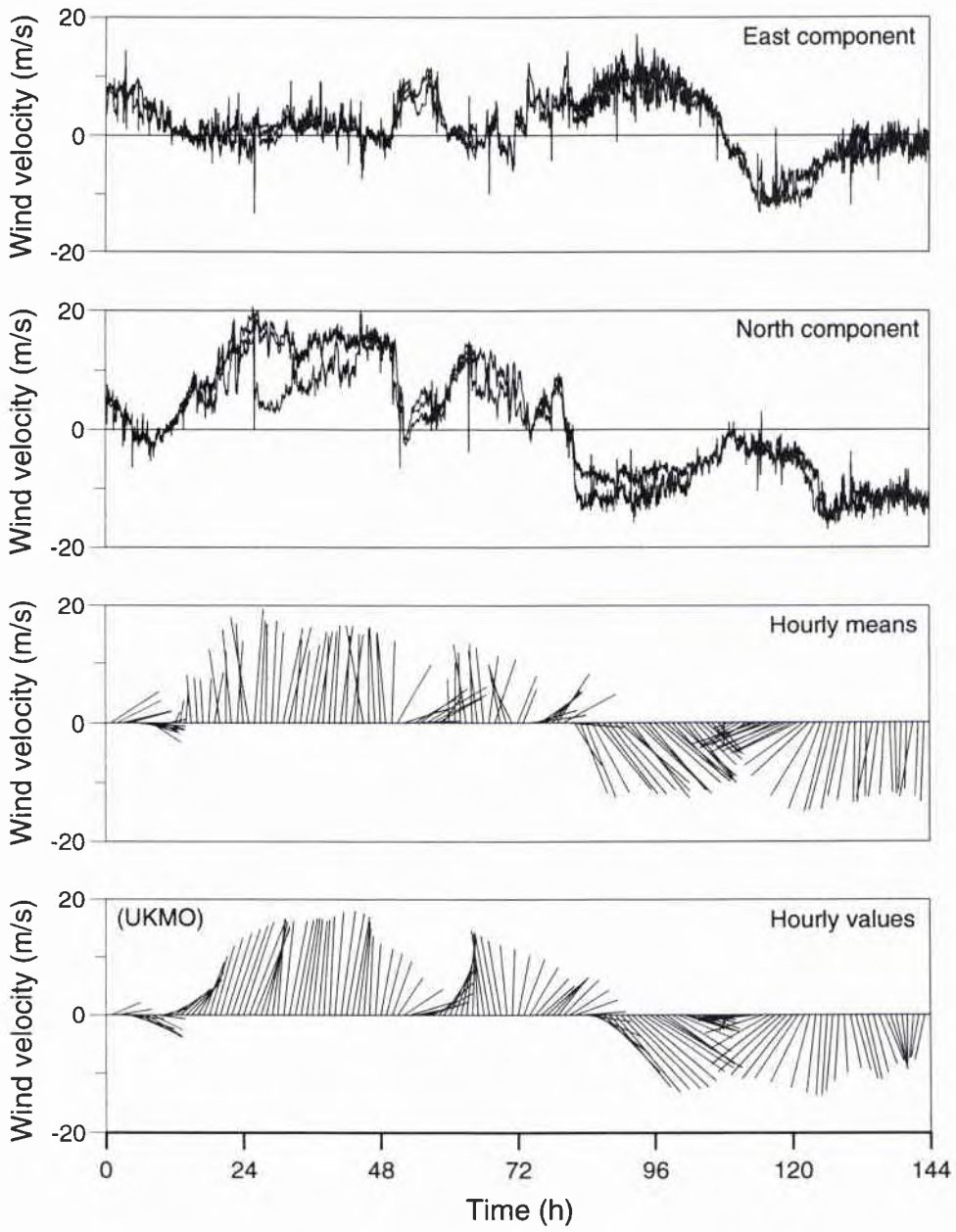

Figure B6b *Measured and analysed winds from Leg 1b of NORDIC'92a (7 March 1992), for further explanation cf. Fig. 5.2b.*

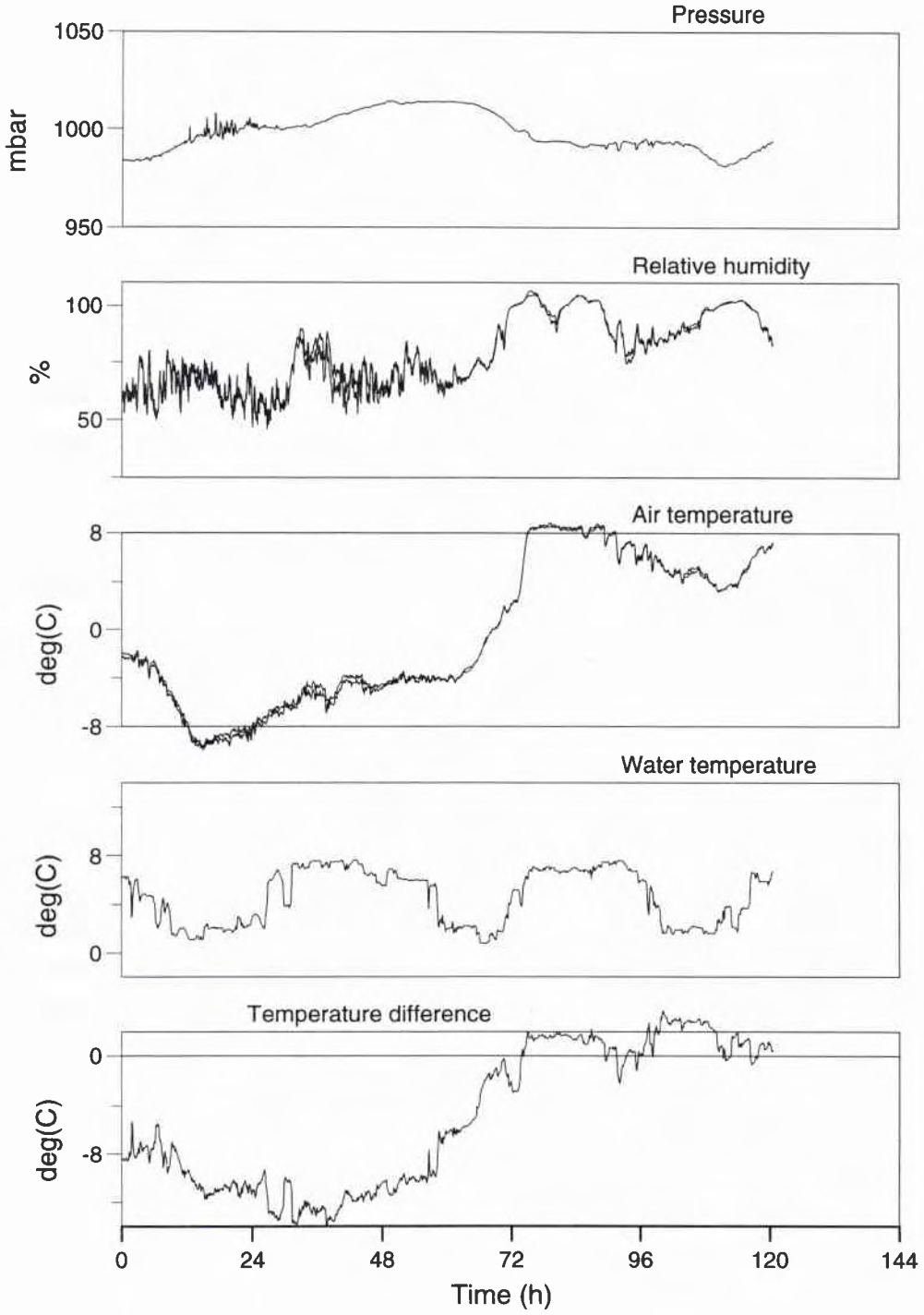

Figure B7a *Surface meteorological data from Leg 1c of NORDIC'92a (13 March 1992), for further explanation cf. Fig. B2a.*

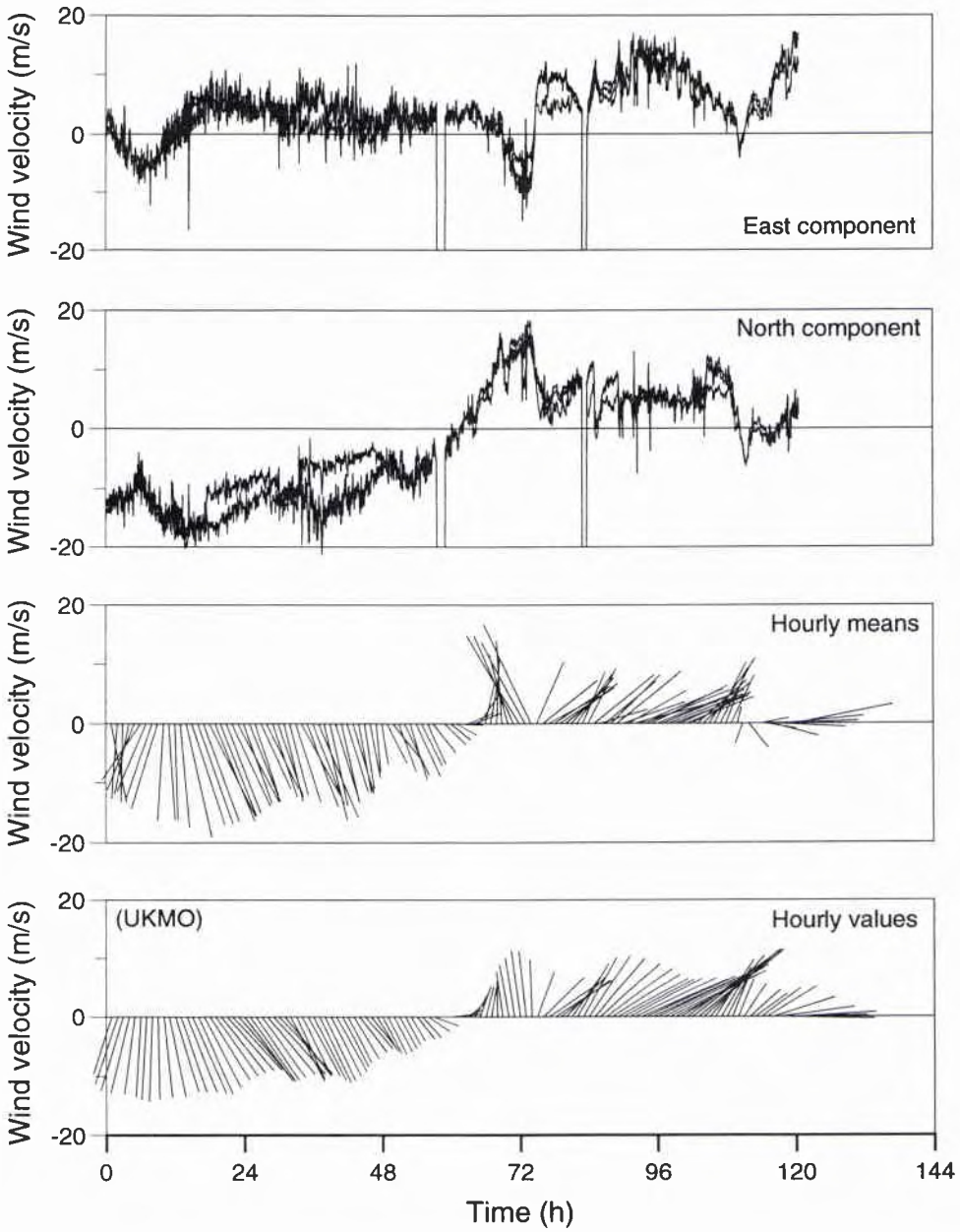

Figure B7b *Measured and analysed winds from Leg 1c of NORDIC'92a (13 March 1992), for further explanation cf. Fig. B2b.*

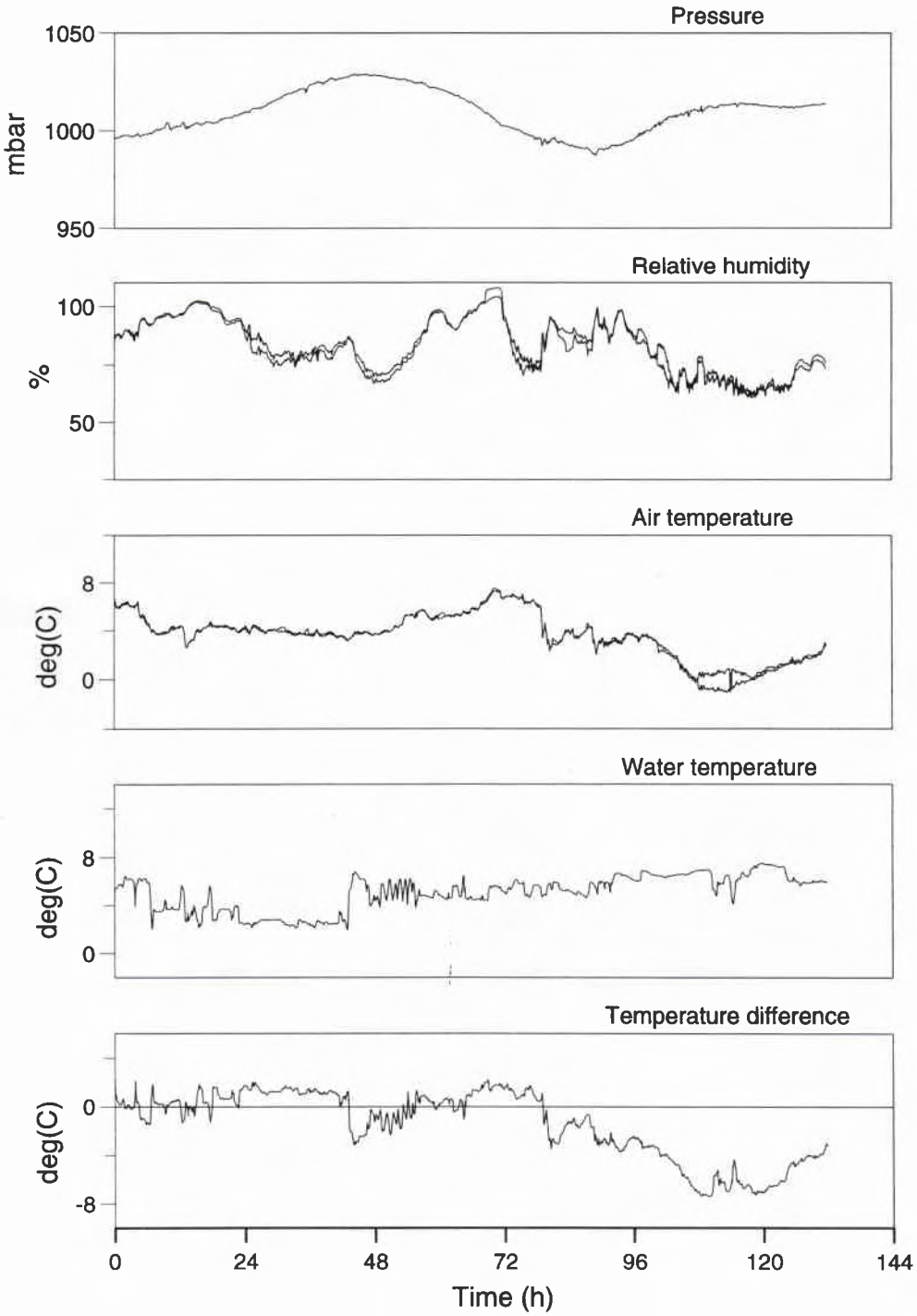

Figure B8a *Surface meteorological data from Leg 2 of NORDIC'92a (22 March 1992), for further explanation cf. Fig. B2a.*

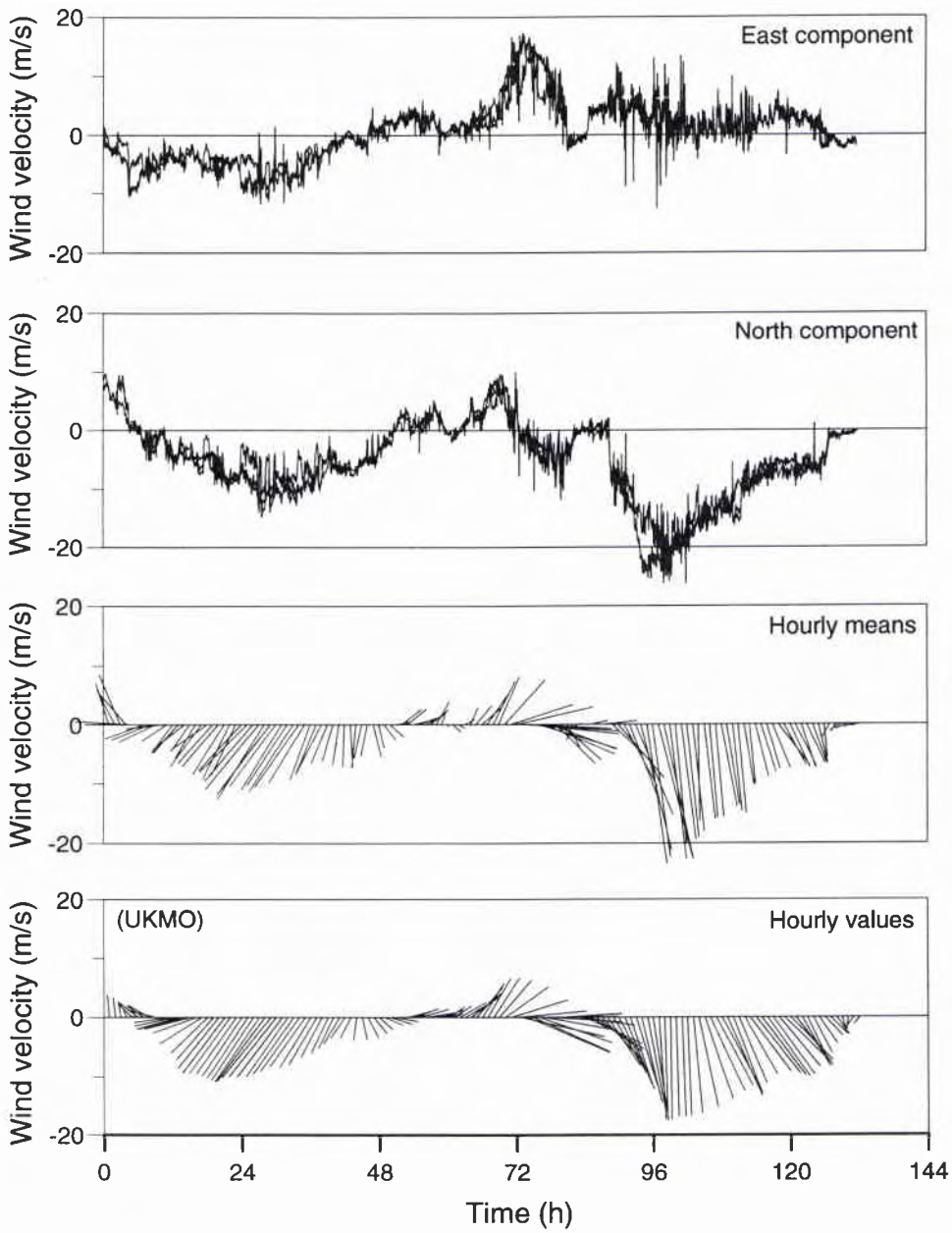

Figure B8b *Measured and analysed winds from Leg 2 of NORDIC'92a (22 March 1992), for further explanation cf. Fig. B2b.*

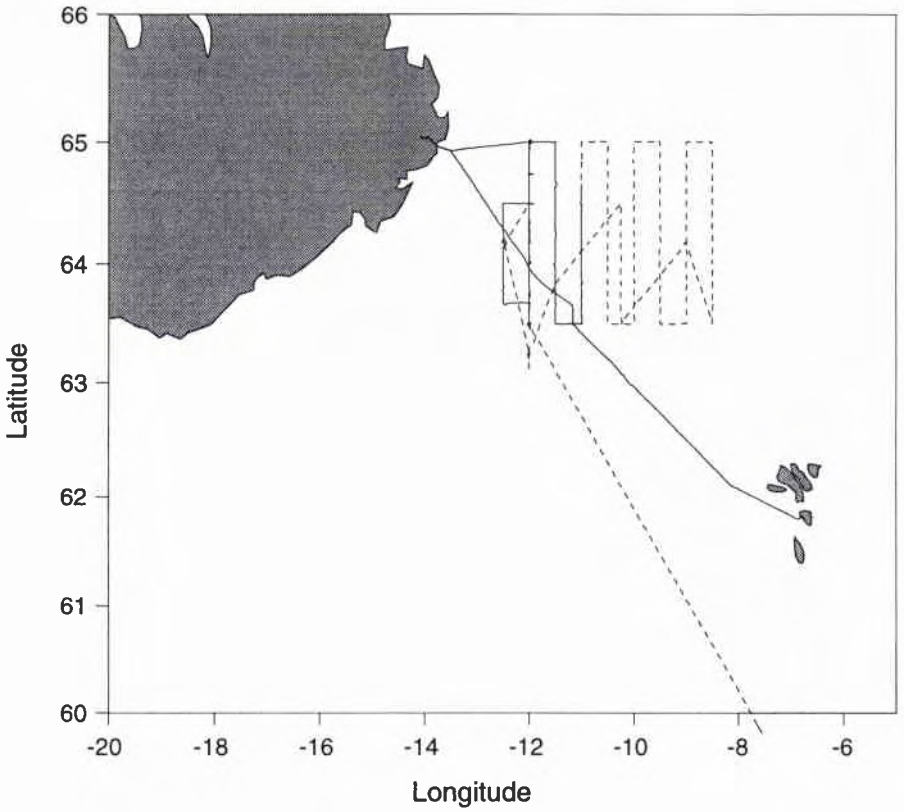

Figure B9 *Track of R/V Alliance during NORDIC'92b: Leg 1a (solid line) – from 16 October 1992, 0:00 to 21 October 1992, 24:00; Leg 1b (dashed line) – from 22 October 1992, 0:00 to 27 October 1992, 24:00.*

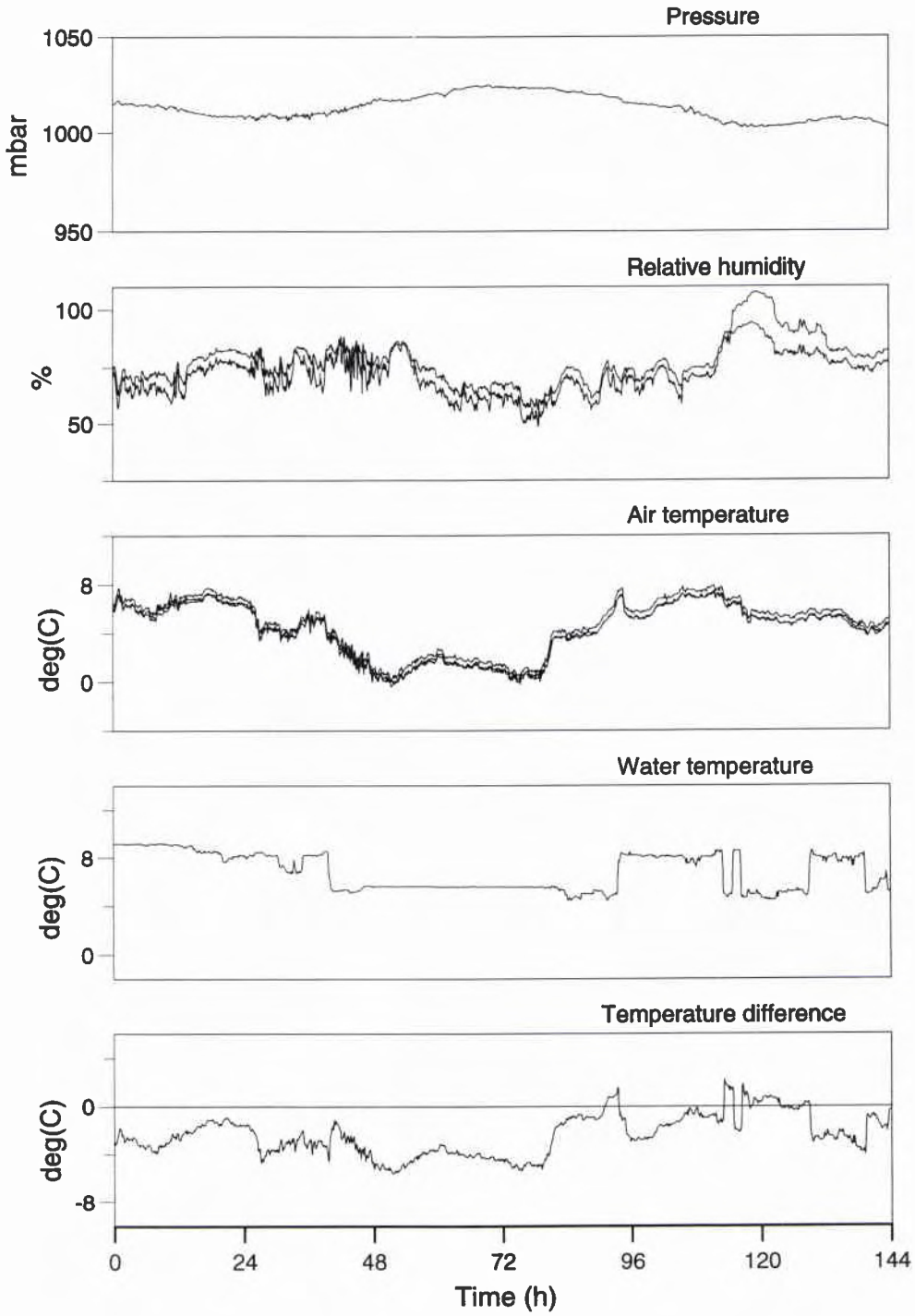

Figure B10a *Surface meteorological data from Leg 1a of NORDIC'92b (16 October 1992), for further explanation cf. Fig. B2a.*

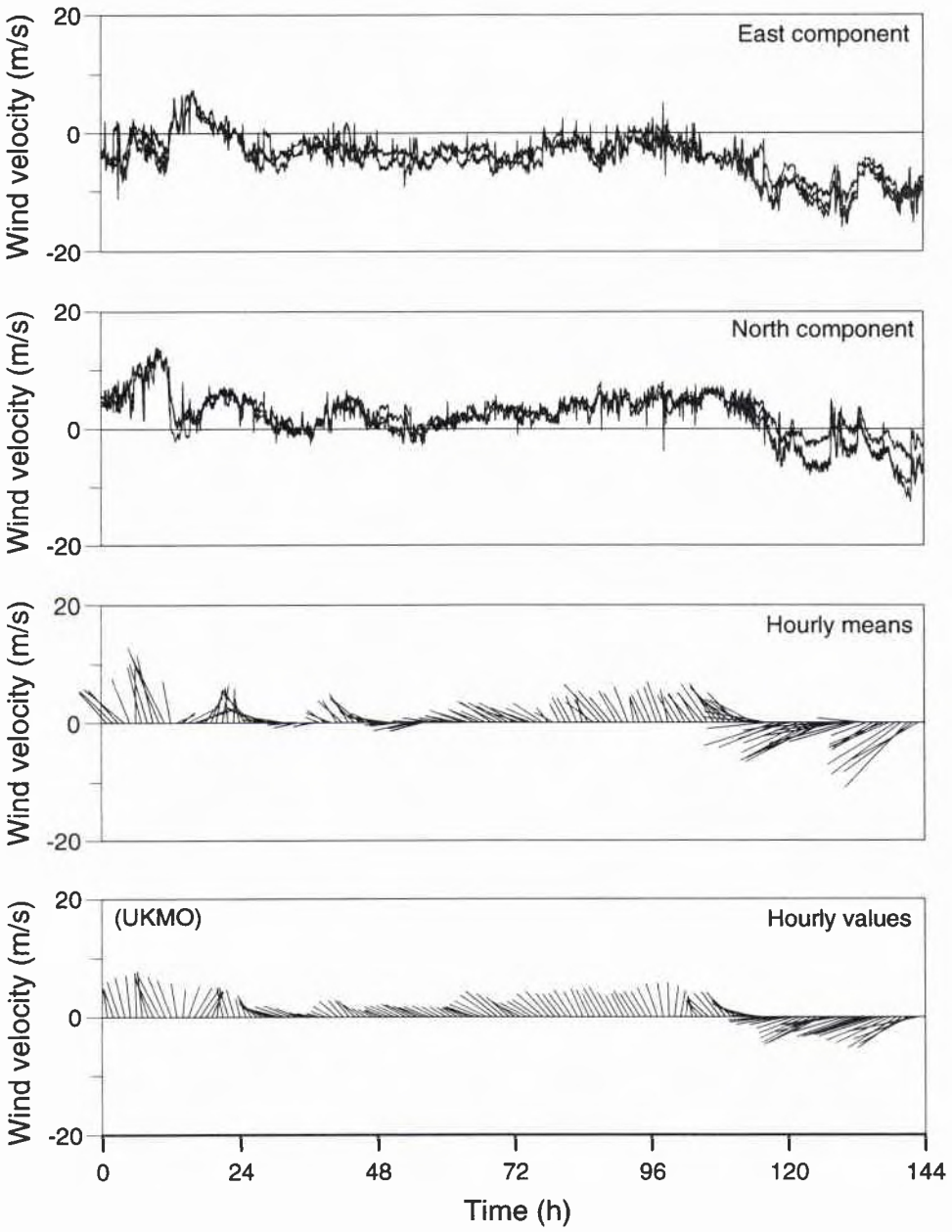

Figure B11b *Measured and analysed winds from Leg 1b of NORDIC'92b (22 October 1992), for further explanation cf. Fig. B2b.*

Report no. changed (Mar 2006): SR-220-UU

Security Classification		Project No.
NATO UNCLASSIFIED		23
Document Serial No.	**Date of Issue**	**Total Pages**
SR-220	April 1994	60 pp.

Author(s)

H.-H. Essen

Title

Sea-surface winds in the Iceland–Faeroe area, as derived from the ERS-1 scatterometer

Abstract

This report presents measurements of surface meteorological data taken during three cruises of R/V *Alliance* to the Iceland–Faeroe frontal area during August 1991 (NORDIC'91), March 1992 (NORDIC'92a) and October 1992 (NORDIC'92b). Wind velocity and direction, as measured at three different locations on the ship, are compared with wind information retrieved from the scatterometer of the European Remote Sensing Satellite (ERS-1). As coincident *in situ* and satellite measurements are relatively rare, analysed winds from the UK Meteorological Office are also used for comparison. For the satellite data, different retrieval algorithms are applied. Beside the wind vector, its horizontal derivatives (e.g. horizontal divergence and curl) are also investigated.

Keywords

ERS-1, Iceland–Faeroe area, microwave radar, satellite remote sensing, scatterometer, sea-surface winds

Issuing Organization

North Atlantic Treaty Organization
SACLANT Undersea Research Centre
Viale San Bartolomeo 400, 19138 La Spezia, Italy

tel: 0187 540 111
fax: 0187 524 600
telex: 271148 SACENT I

[From N. America: SACLANTCEN CMR-426 (New York) APO AE 09613]

Report no. changed (Mar 2006): SR-220-UU

Initial Distribution for SR-220

Ministries of Defence	
JSPHQ Belgium	2
DND Canada	10
CHOD Denmark	8
MOD France	8
MOD Germany	15
MOD Greece	11
MOD Italy	10
MOD Netherlands	12
CHOD Norway	10
MOD Portugal	5
MOD Spain	2
MOD Turkey	5
MOD UK	20
SECDEF US	54
NATO Authorities	
NAMILCOM	2
SACLANT	3
CINCIBERLANT	1
COMSUBACLANT	1
COMNAVSOUTH	1
SCNR for SACLANTCEN	
SCNR Belgium	1
SCNR Canada	1
SCNR Denmark	1
SCNR Germany	1
SCNR Greece	1
SCNR Italy	1
SCNR Netherlands	1
SCNR Norway	1
SCNR Portugal	1
SCNR Spain	1
SCNR Turkey	1
SCNR UK	1
SCNR US	2
French Delegate	1
SECGEN Rep. SCNR	1
NAMILCOM Rep. SCNR	1
National Liaison Officers	
NLO Belgium	1
NLO Canada	1
NLO Denmark	1
NLO Germany	1
NLO Italy	1
NLO Netherlands	1
NLO UK	1
NLO US	1
Total external distribution	205
SACLANTCEN Library	20
Total number of copies	225